國立交通大學

電子工程學系 電子研究所碩士班

碩士論文

適用於多輸入多輸出系統之

低複雜度與改善性能之方法

Reducing Complexity and Improving Performance

Techniques for LDPC-Coded MIMO Systems
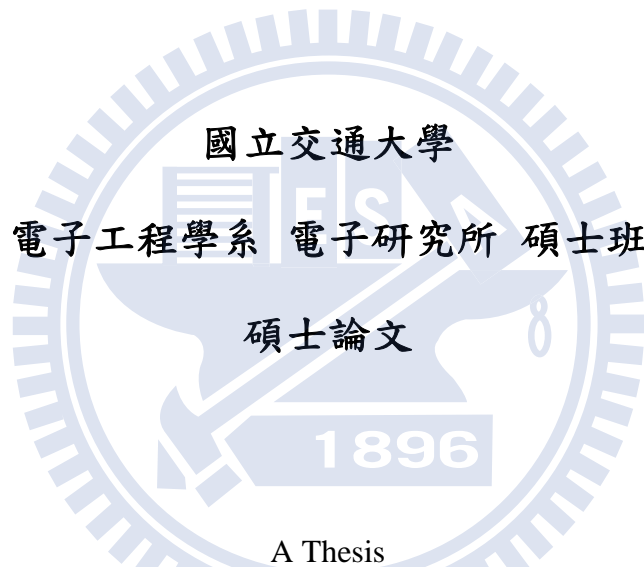
研究生：劉玉婷

指導教授：張錫嘉 博士

中華民國 九十九 年 九 月

適用於多輸入多輸出系統之

低複雜度與改善性能之方法

Reducing Complexity and Improving Performance

Techniques for LDPC-Coded MIMO Systems

研究生　　：劉玉婷　　　　　　　　Student : Liu-Yu Ting

指導教授：張錫嘉　博士　　　　　　Advisor : Dr. Hsie-Chia Chang

國立交通大學

電子工程學系　電子研究所　碩士班

碩士論文

A Thesis

Submitted to Department of Electronics Engineering & Institute Electronics

College of Electrical and Computer Engineering

National Chiao Tung University

In Partial Fulfillment of the Requirements

for the Degree of

Master of Science

in

Electronics Engineering

September 2010

Hsinchu, Taiwan, Republic of China

中 華 民 國　九 十 九　年　九　月

適用於多輸入多輸出系統之

低複雜度與改善性能之方法

學生：劉玉婷　　　　　　　指導教授：張錫嘉 博士

國立交通大學

電子工程學系　　電子研究所碩士班

摘要

多輸入多輸出天線系統（Multiple Input and Multiple Output，簡稱MIMO）因為擁有更佳的傳輸效率及訊號的品質，所以被廣泛的應用在無線通訊的系統中。通道解碼使得整個系統在低訊雜比的環境中可以有較佳的表現。因此在目前所使用的許多規格中如IEEE802.11n、IEEE802.16e和3GPP LTE，會將多輸入多輸出天線系統在接收端訊號偵測與通道解碼做連接。其中因為規格的需求，通道編碼是利用低密度奇偶校驗碼（Low Density Parity Check，簡稱LDPC Codes）或渦輪解碼（Turbo Decoding），為了得到較好的表現，在MIMO的訊號偵測中需要產生軟輸出。然而，在產生軟輸出的過程中會使得整體解碼複雜度的提升，因此，本篇論文提出可以降低複雜度的演算法，並提出可以更加改善傳統MIMO訊號偵測錯誤率的兩種技巧。

首先，在本篇論文中提出雙方向演算法（Bi-direction），利用兩次的QR分解去做成本的計算，與QOC的方法相比，運算量最多可以減少30 %。接著透過非線性量化的方法（Nonlinear Quantization），把MIMO訊號偵測的軟輸出做分佈上的改變，使得錯誤率最大可以達到2dB的改善。最後，運用二階段（Two-stage）的技巧，在第一階段維持原來LDPC的解碼，在第二階段將一些不可靠的位元做數值的翻轉，在MIMO與LDPC連接的系統中，錯誤率最大可以達到0.3dB的改善。

Reducing Complexity and Improving Performance Techniques for LDPC-Coded MIMO Systems

Student : Yu-Ting Liu   Advisor : Hsie-Chia Chang

Department of Electronics Engineering

Institute of Electronics

National Chiao Tung University

Abstract

This thesis proposes three approaches to apply for the channel-coded MIMO system. MIMO communication system has been widely applied in many wireless communications for better transmission efficiency and signal quality. Channel coding or forward error correction allows the system work better with the additional coding gain in lower SNR environment. Channel-coded MIMO system which refers to the MIMO detection with channel coding scheme is defined in many communication standard such as IEEE802.11n, IEEE802.16e and 3GPP LTE. Soft-output of MIMO system is required to a concatenate channel coding like turbo code and low-density parity-check (LDPC). However, complexity increases intensively as the hard-outputs transfer to soft-outputs of MIMO detection.

A bi-direction method to reduce the complexity of soft-output MIMO decoding is proposed in this thesis. Sphere decoding of MIMO system encounters the empty-set issue as generating LLRs. Bi-direction method solves the empty-set issue and reduce the computations at most 30% compared to the original method QOC. In addition, nonlinear quantization (NLQ) is applied to the list sphere decoding and obtains a great performance improvement at most 2dB with little computation complexity. Furthermore, a two-stage algorithm applied on the channel-coded MIMO system is presented to improve the error performance at most 0.3dB.

誌 謝

Contents

List of Figures

List of Tables

v

Chapter 1

Introduction

1.1 Motivation

Multiple-input multiple-out (MIMO) technoloy is widely recognized as the future wireless communication systems, and it's becoming an essential part in the new wireless standard [1], [2]. MIMO systems can be used to improve the transmission quality by sending the same data which is referred as spatial diversity, or to increase the channel capacity by transmitting different data which is called spatial multiplexing [3]. There are several methods to detect the signals at the receiver [4], [5], [6]. *Maximum-likelihood* (ML) performs the best error performance for minimizing the symbol error probabilities. However, the exhaustic search is infeasible since it requires huge computation complexity with the growth of the number of antenna and the size of constellation. *Sphere decoding* (SD) algorithm can be applied as an efficient means to searching for the sequence with the minimum path metric. Instead of exhaustively search, only the signals within the radius will be searched in SD. However, the computation complexity depends on the channel conditions and the noise variance, and the non-constant decoder throughput results to difficulties in hardware implementation. Thus, K-best SD [7], [8] is often used as an alternative approximation and K should be large enough to guarantee ML performance. For the channel-coded MIMO system, soft ouputs of MIMO detector are required and an empty-set issue has to be dealt with. Therefore, the list size is a tradeoff between error performance and computation complexity.

In this thesis, a bi-direction method is proposed to reduce the computation complexity

when the MIMO decoder generates the soft outputs. A nonlinear quantization method to improve the error performance of list sphere decoding is discussed. Furthermore, a two-stage algorithm applied on the channel-coded MIMO system is presented to improve the error performance.

1.2   Thesis Organization

Complexity reduction and the trade-off between performance for designing sphere decoders and LDPC decoders are the focus of this dissertation.The dissertation can be organized as follows. In Chapter 2, MIMO system models are introduced, and several MIMO signal detection methods are briefly reviewed. Then, the bi-direction algorithms is presented in Chapter 3, including parameters derivations and complexity analysis. A two-stage algorithm is presented in Chapter 4 for the channel-coded MIMO system. Subsequently, the simulation results are given in Chapter 5. Finally, Chapter 6 concludes this work.
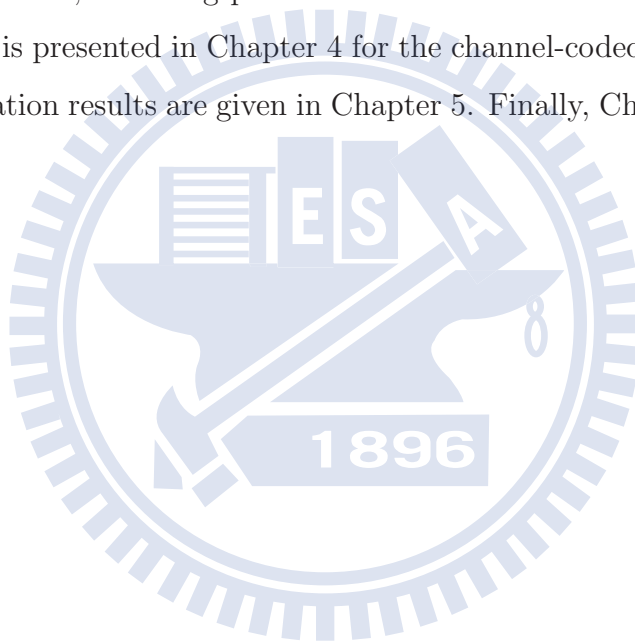
Chapter 2

MIMO System

MIMO communication system has been widely applied in many wireless communications. This is an approach to achieve better transmission efficiency and signal quality due to the spatial multiplexing and the inherent diversity gain. Diversity gain refers to the slope of the error probability vesus SNR plot in a log-scale. Diversity provides multiple paths to manage fading channel and thus boost the system capacity. When the system spatial multiplexing strategy and the signal detection schemes are given, the maximum achievable diversity gain is determined [9]. In the following, a brief review of MIMO system and the channel models will be given first, and several linear and non-linear MIMO detection schemes will be introduced later.
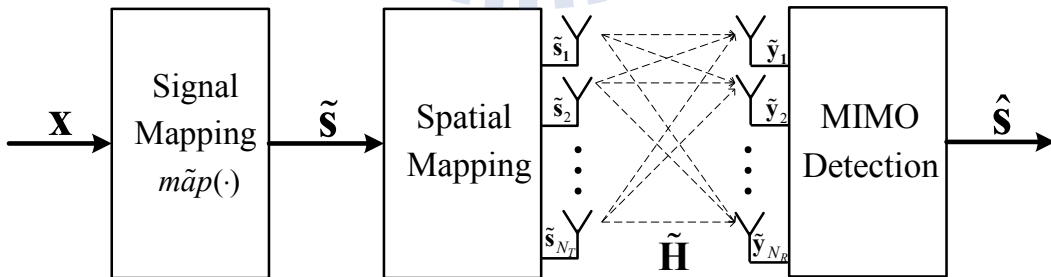
2.1 System Model

Figure 2.1: Simplified MIMO system model

Fig. 2.1 illustrates a simplified MIMO system model. A bit stream $\mathbf{x}$ map to a symbol

3

steam by the signal mapping function $map(\cdot)$, such as PSK and QAM modulation. Then the symbols $\tilde{\mathbf{s}}$ are transmitted by the different antennas which are decided by the spatial mapping method. At the receiver, $\tilde{\mathbf{y}}$ is the received vector which is interfered by the channel and noise and $\hat{\mathbf{s}}$ is the decoding output that is detected by the MIMO detection.

In the mathematical representation, a MIMO system of N_T transmit antennas and N_R receive antennas can be represented by

$$\tilde{\mathbf{y}} = \tilde{\mathbf{H}}\tilde{\mathbf{s}} + \tilde{\mathbf{n}}, \tag{2.1}$$

where $\tilde{\mathbf{s}}$ is the $N_T \times 1$ transmitted signal vector, $\tilde{\mathbf{H}}$ is an $N_T \times N_R$ channel matrix of independent and identical distributed (i.i.d.) complex Gaussian elements, and $\tilde{\mathbf{n}}$ is an $N_R \times 1$ i.i.d. complex Gaussian noise vector, and $\tilde{\mathbf{y}}$ is the $N_R \times 1$ received signal. Note that an independent and flat-fading channel is assumed in (2.1). For convenience, there is a simplified method referred to the *real value decomposition*. Thus, (2.1) is often represented by an equivalent real-valued form as

$$\begin{aligned}
\mathbf{y} &= \begin{bmatrix} \Re\{\tilde{\mathbf{y}}\} \\ \Im\{\tilde{\mathbf{y}}\} \end{bmatrix} \\
&= \begin{bmatrix} \Re\{\tilde{\mathbf{H}}\} & -\Im\{\tilde{\mathbf{H}}\} \\ \Im\{\tilde{\mathbf{H}}\} & \Re\{\tilde{\mathbf{H}}\} \end{bmatrix} \begin{bmatrix} \Re\{\tilde{\mathbf{s}}\} \\ \Im\{\tilde{\mathbf{s}}\} \end{bmatrix} + \begin{bmatrix} \Re\{\tilde{\mathbf{n}}\} \\ \Im\{\tilde{\mathbf{n}}\} \end{bmatrix} \\
&= \mathbf{Hs} + \mathbf{n}.
\end{aligned} \tag{2.2}$$

where $\Re\{\cdot\}$ and $\Im\{\cdot\}$ respectively refer to the real and the imaginary parts of a complex signal. The complex modulation $map(\cdot)$ also decomposed into two real-valued singnal mapping $map(\cdot)$. For example, M^2-QAM mapping is transformed to two M-PAM modulation. Futhermore, the channel matrix $\tilde{\mathbf{H}}$ is assumed to have full rank and to be perfectly estimated at the receiver.

2.2 MIMO Signal Detection Algorithm

MIMO signal detection can be classified into linear detection and nonlinear detection. Linear equalization and successive interference cancellation are two representative approaches in the linear category. For nonlinear detection, maximum-likelihood detection can achieve optimum performance with the expense of higher computation complexity. There are several detection methods in the following.

2.2.1 Linear Detection Methods

Linear detection methods try to compensate received signal by equalizing the channel response. *Zero-forcing* (ZF) and *minimum mean-squared error* (MMSE) [10] equalizations are the two most common linear schemes. Assume the pseudo-inverse channel matrix is $\tilde{\mathbf{H}}^+ = (\tilde{\mathbf{H}}^H \tilde{\mathbf{H}})^{-1} \tilde{\mathbf{H}}^H$. When $N_T = N_R$, $\tilde{\mathbf{H}}^+ = \tilde{\mathbf{H}}^{-1}$, that is, the inverse of the channel matrix.

ZF equalization can be realized by directly multiplying the received vector $\tilde{\mathbf{y}}$ by $\tilde{\mathbf{H}}^+$; therefore,

$$\tilde{\mathbf{H}}^+ \tilde{\mathbf{y}} = \tilde{\mathbf{H}}^+ (\tilde{\mathbf{H}} \tilde{\mathbf{s}} + \tilde{\mathbf{n}}) = \tilde{\mathbf{s}} + \tilde{\mathbf{H}}^+ \tilde{\mathbf{n}} \tag{2.3}$$

The ZF solution can be derived by quantizing $\tilde{\mathbf{H}}^+ \tilde{\mathbf{y}}$ to its nearest integers. It provides the maximum achievable diversity gain is $N_R - N_T - 1$ [9]. However, the noise is enhanced by $\tilde{\mathbf{H}}^+$ and limits the system performance.

MMSE equalization aims to substitute the $\tilde{\mathbf{H}}^+$ in (2.3) by other compensation matrix such that the average enhanced noise power is minimized. Given ρ as the received SNR, the MMSE equalization estimates $\tilde{\mathbf{s}}$ by multiplying $\tilde{\mathbf{y}}$ with

$$\mathbf{D_{MMSE}} = (\frac{\mathbf{I_{N_r}}}{\rho} + \tilde{\mathbf{H}}^H \tilde{\mathbf{H}})^{-1} \tilde{\mathbf{H}}^H \tag{2.4}$$

The MMSE receiver has the same maximum diversity as the ZF receiver, which is $N_R - N_T - 1$ [9]. Although linear detections require lower complexity, the performance degradation is significant.

2.2.2 Successive Interference Canceling

The MIMO system model in (2.1) can be rewritten as

$$\begin{aligned} \tilde{\mathbf{y}} &= \sum_{i=1}^{N_T} \tilde{\mathbf{h}}_i \tilde{\mathbf{s}}_i + \tilde{\mathbf{n}} \\ &= \tilde{\mathbf{h}}_k \tilde{\mathbf{s}}_k + \sum_{i=1, i \neq k}^{N_T} \tilde{\mathbf{h}}_i \tilde{\mathbf{s}}_i + \tilde{\mathbf{n}}, \end{aligned} \tag{2.5}$$

where $\tilde{\mathbf{h}}_i$ refers to the i-th column of the channel matrix $\tilde{\mathbf{H}}$. The second element of (2.5) is regarded as interference to $\tilde{\mathbf{s}}_k$. *Successive interference cancelling* (SIC) tries to estimate the partial symbols to remove the interference.

SIC detection have N_T stages and assume $\tilde{\mathbf{s}}_k$ detects at the k-th stage. Supposed $\hat{\mathbf{s}}_1, \hat{\mathbf{s}}_2, \ldots, \hat{\mathbf{s}}_{k-1}$ be the estimates of $\tilde{\mathbf{s}}_1, \tilde{\mathbf{s}}_2, \ldots, \tilde{\mathbf{s}}_{k-1}$. Substracting the estimates from $\tilde{\mathbf{y}}$, then received vector $\tilde{\mathbf{y}}_k$ is

$$\tilde{\mathbf{y}}_k = \tilde{\mathbf{y}} - \sum_{i=1}^{k-1} \tilde{\mathbf{h}}_i \hat{\mathbf{s}}_i + \tilde{\mathbf{n}}. \tag{2.6}$$

Since the interference from $\tilde{\mathbf{s}}_1, \tilde{\mathbf{s}}_2, \ldots, \tilde{\mathbf{s}}_{k-1}$ is deleted. Then interference nulling restrains the rest interference from $\tilde{\mathbf{s}}_{k+1}, \tilde{\mathbf{s}}_{k+2}, \ldots, \tilde{\mathbf{s}}_{N_T}$. The nulling process is similar to ZF and MMSE equalization. Apparently, SIC suffers from error propagation if the first few symbols are detected incorrectly. Therefore, *ordered successive interference cancellation* (OSIC) or *Bell Lab layered space-time* (BLAST) [11] is brought out to sort the detection order. The maximum achievable diversity gain of SIC is $N_R - N_T + k$ [9]. Although the performance is better than ZF and MMSE, the performance is still suboptimal. There is a optimal solution of MIMO detection and will be introduced in the next section.

2.2.3   Maximum-likelihood Signal Detection

Maximum-likelihood (ML) signal detection is one of the optimal detection method in the MIMO system. ML estimates the transmit vector $\tilde{\mathbf{s}}$ by searching for a vector $\hat{\mathbf{s}}$ that maximizes the conditional probability,

$$\hat{\mathbf{s}} = \arg \max_{\mathbf{s} \in \mathbf{\Omega}^{N_t}} Pr(\tilde{\mathbf{y}}|\mathbf{s}), \tag{2.7}$$

where Ω denotes all possible constellation points of the mapping function $map(\cdot)$. According to the Gaussian system model in (2.1) and the equivalent real-valued form in (2.2), (2.7) can be reduced to a closet-lattice-point searching problem [12],

$$\hat{\mathbf{s}}_{ML} = \arg \min_{\mathbf{s} \in \mathbf{\Omega}^{2N_t}} \|\mathbf{y} - \mathbf{H}\mathbf{s}\|^2, \tag{2.8}$$

where $\mathbf{s}$ is an $2N_T$ dimensional lattice point of the lattice generated by $\tilde{\mathbf{H}}$, $\|\mathbf{a}\|^2 = \sum_{i=1}^{N} (a_i)^2$ denotes the Euclidian norm of N-dimensional vector $\mathbf{a}$, and $\mathbf{\Omega}^{2N_t} = \mathbf{\Omega} \times \mathbf{\Omega} \times \cdots \times \mathbf{\Omega}$ the $2N_T$ times Cartesian product of Ω. That is, ML detection is to find a vector $\mathbf{s}$ over the combination of $\mathbf{\Omega}^{2N_t}$ that minimize $\|\mathbf{y} - \mathbf{H}\mathbf{s}\|^2$. ML detection has been proved that fully utilizes the benefit of diversity, N_R, but the computation complexity is exponential growth with $N_T \times |\Omega|$. Therefore, a detection algorithm to realize ML detection while decreasing the complexity is essential. In the following, the sphere decoding algorithm will be introduced.

2.3 Sphere Decoding Algorithm

From the previous section, the computation complexity and the performance are increased in an order by ZF, MMSE, ZF-SIC, MMSE-SE, ML. Although ML detection is the optimal solution, exhaustively search for minimum of (2.8) to realize it is infeasible when number of antennas and the constellation grow. Therefore, there are some simplied search strategies to realize ML dectection. Following are depth-first and breath-first sphere decoding(SD) introduced to reduce the complexity.

2.3.1 Depth First Sphere Decoding

The sphere decoding searches for the minimizer in the hypersphere, which is $\|\mathbf{y} - \mathbf{Hs}\|^2 \leq R$. Assume R is choosing properly such that the sphere contains at least one lattice point, (2.8) becomes

$$\hat{\mathbf{s}}_{ML} \approx= \hat{\mathbf{s}}_{SD} = \arg \min_{\mathbf{s} \in \mathbf{\Omega}^{2N_t}, \|\mathbf{y} - \mathbf{Hs}\|^2 \leq r^2} \|\mathbf{y} - \mathbf{Hs}\|^2, \tag{2.9}$$

Fig. 2.2 depicts the simple concept of sphere decoding. Take $N_T = 1$ and 16-QAM into account, SD algorithm searches the candidates in the circle and pruning the rest constellation points outside the radius. And the solution is the lattice point that is the closest to the received signal.
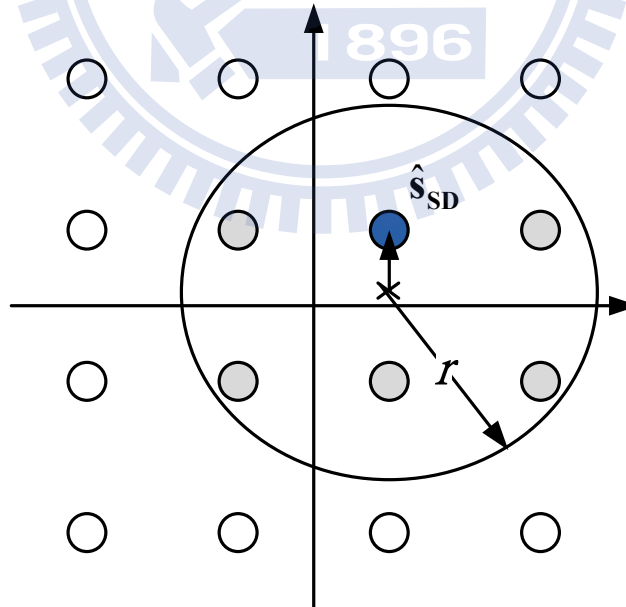

Figure 2.2: Geometrical representation of sphere decoding algorithm

In addition, (2.9) converts the closest-search problem to a tree-search problem while preprocessing technique is applied. By QR-decomposition, the channel matrix is factorizd to $\mathbf{H} = \mathbf{Q}\mathbf{R}$ and $\mathbf{Q}$ is an $2N_R \times 2N_T$ unitary matrix and $\mathbf{R}$ is an $2N_T \times 2N_T$ upper triangular matrix. Multiplying $\mathbf{y}$ by $\mathbf{Q}^T$, (2.9) transforms to

$$\hat{\mathbf{s}}_{SD} = \arg \min_{\mathbf{s} \in \mathbf{\Omega}^{2N_t}, \|\mathbf{y} - \mathbf{R}\mathbf{s}\|^2 \leq r^2} \|\hat{\mathbf{y}} - \mathbf{R}\mathbf{s}\|^2, \tag{2.10}$$

where $\hat{\mathbf{y}} = \mathbf{Q}^T \mathbf{y}$.

Due to the triangular form of matrix $\mathbf{R}$, the vector form of (2.10) is

$$
\begin{aligned}
\hat{\mathbf{s}} &= \arg \min_{\mathbf{s} \in \mathbf{\Omega}^{N_T}, \|\hat{\mathbf{y}} - \mathbf{H}\mathbf{s}\|^2 \leq r^2} \sum_{i=1}^{2N_T} \left(\hat{y}_i - \sum_{j=i}^{2N_T} R_{ij} s_j^{(i)} \right)^2 \\
&= \arg \min_{\mathbf{s} \in \mathbf{\Omega}^{N_T}, \|\hat{\mathbf{y}} - \mathbf{H}\mathbf{s}\|^2 \leq r^2} \sum_{i=1}^{2N_T} e(\mathbf{s}^{(i)}),
\end{aligned} \tag{2.11}
$$

where the *partial path* is $\mathbf{s}^{(i)} = [s_i^{(i)} s_{i+1}^{(i)} \cdots s_{2N_T}^{(i)}]^T$. The *partial Euclidean distance* (PED) of $\mathbf{s}^{(i)}$ is defined as

$$
\begin{aligned}
T(\mathbf{s}^{(i+1)}) &= \sum_{i'=i}^{2N_T} \left(\hat{y}_{i'} - \sum_{j=i'}^{2N_T} R_{i'j} s_j^{(i')} \right)^2 \\
&= \sum_{i'=i+1}^{2N_T} \left(\hat{y}_{i'} - \sum_{j=i'}^{2N_T} R_{i'j} s_j^{(i')} \right)^2 + \left(\hat{y}_i - \sum_{j=i}^{2N_T} R_{ij} s_j^{(i)} \right)^2 \\
&= T(\mathbf{s}^{(i+1)}) + e(\mathbf{s}^{(i)}).
\end{aligned} \tag{2.12}
$$

From (2.12), the tree search algorithm initiates from $2N_T$-th layer, which denotes *root node*, to the 1-st layer of the tree, which indicates *leaf note*. According to (2.10) and (2.11), SD searches the lattice points in the hypersphere, that is, satisfy the radius constraint,

$$
\begin{aligned}
r^2 &\geq \sum_{i=1}^{2N_T} \left(\hat{y}_i - \sum_{j=i}^{2N_T} R_{ij} s_j^{(i)} \right)^2 \\
&= (\hat{y}_{2N_T} - R_{2N_T, 2N_T} s_{2N_T})^2 \\
&+ (\hat{y}_{2N_T-1} - R_{2N_T-1, 2N_T-1} s_{2N_T-1} - R_{2N_T-1, 2N_T} s_{2N_T})^2 \\
&\vdots \\
&+ (\hat{y}_1 - R_{1,1} s_1 - R_{1,2} s_2 - \cdots - R_{1, 2N_T} s_{2N_T})^2.
\end{aligned} \tag{2.13}
$$

Fig. 2.3 describes the simplied searching strategy of SD. Consider $N_T = 2$, BPSK MIMO system, the nodes on the blue paths passes the radius constraint, which means the paths are the possible candidates and the rest paths are discarded.
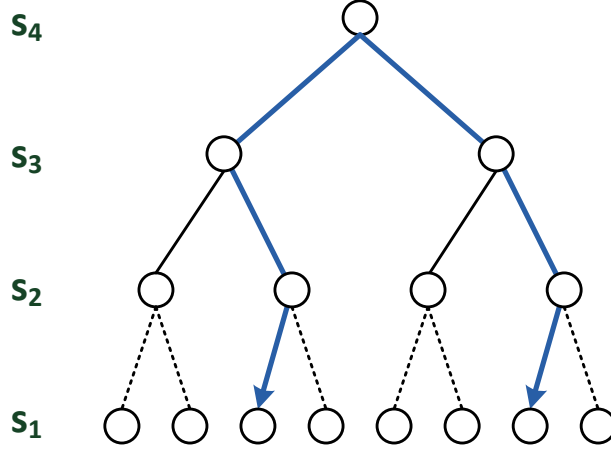

Figure 2.3: Tree-search of sphere decoding

From (2.13), when detection initiates from $2N_T$-th layer, $\mathbf{s}_{2N_T}$ has to satisfy $r^2 \geq (\hat{y}_{2N_T} - R_{2N_T,2N_T} s_{2N_T})^2$. Then,

$$\left\lceil \frac{-r + \hat{y}_{2N_T}}{R_{2N_T,2N_T}} \right\rceil \leq s_{2N_T} \leq \left\lfloor \frac{r + \hat{y}_{2N_T}}{R_{2N_T,2N_T}} \right\rfloor, \tag{2.14}$$

and define the lower bound

$$L_{2N_T} = \left\lceil \frac{-r + \hat{y}_{2N_T}}{R_{2N_T,2N_T}} \right\rceil, \tag{2.15}$$

and the upper bound

$$U_{2N_T} = \left\lfloor \frac{r + \hat{y}_{2N_T}}{R_{2N_T,2N_T}} \right\rfloor. \tag{2.16}$$

At $2N_T - 1$-th layer, define $r_{2N_T-1}^2 = r^2 - (\hat{y}_{2N_T} - R_{2N_T,2N_T} s_{2N_T})^2$, then (2.9) becomes

$$r_{2N_T-1}^2 \geq (\hat{y}_{2N_T-1} - R_{2N_T-1,2N_T-1} s_{2N_T-1} - R_{2N_T-1,2N_T} s_{2N_T})^2. \tag{2.17}$$

Besides, define

$$\hat{y}_{2N_T-1|2N_T} = \hat{y}_{2N_T-1} - R_{2N_T-1,2N_T} s_{2N_T}. \tag{2.18}$$

Therefore,

$$L_{2N_T-1} = \left\lceil \frac{-r_{2N_T-1} + \hat{y}_{2N_T-1|2N_T}}{R_{2N_T-1,2N_T-1}} \right\rceil \leq s_{2N_T-1} \leq \left\lfloor \frac{r_{2N_T-1} + \hat{y}_{2N_T-1|2N_T}}{R_{2N_T-1,2N_T-1}} \right\rfloor = U_{2N_T-1}. \tag{2.19}$$

In the simliar process, the candidates from $2N_T - 2$-th layer to 1-th layer can be derived recursively from

$$L_k = \left\lceil \frac{-r_k + \hat{y}_{k|k+1}}{R_{k,k}} \right\rceil \leq s_k \leq \left\lfloor \frac{r_k + \hat{y}_{k|k+1}}{R_{k,k}} \right\rfloor = U_k, \tag{2.20}$$

where

$$\hat{y}_{k|k+1} = \hat{y}_k - \sum_{i=k+1}^{2N_T} R_{ki} s_i^{(k+1)}, \tag{2.21}$$

and

$$r_k^2 = r^2 - T(\mathbf{s}^{(k+1)}). \tag{2.22}$$

The SD algorithm starts from the root node, and the search moves towards to leaf node when the current path metric satisfies the radius upper bound U_k. If the current path metric exceeds U_k, the search moves back to the direction of the root node. Therefore, the search is referred to *depth-first sphere decoding* since the search direction goes back and forth.

Obliviously, the decoding complexity of depth-first sphere decoding depends on the numbers of nodes visited in the searching. At each decoding, the candidates passing the radius constraints, which are referred to *survival paths*, are not constant. Depending on different channels, the throughput of the decoder is not fixed and the decoding direction is not uni-direction. Therefore, this algorithm is not suitable for the hardware implementation. To improve the throughput and apply parallelism and pipeline technique, *breadth-first sphere decoding* arose. This algorithm will be introduced in the following section.

2.3.2 Breadth First Sphere Decoding

Breadth First Sphere Decoding is also called *K-Best SD algorithm*, which is constant decoding throughput and easy to hardware implementation.

The decoding procedure also starts from the root node. Unlike the depth-first search that moves back and forth, K-Best algorithm expands every branch at each layer first and calculates the PEDs of all expanded branches. Secondly, keep K partial paths that the PEDs are smaller and eliminate others. Then, expend the branches of next layer by these K survival partial paths. Perform the iterative steps until reach the leaf node and obtain K survival paths ultimately.

(a) Illustration of depth-first SD (b) Illustration of breadth-first SD and $K = 2$
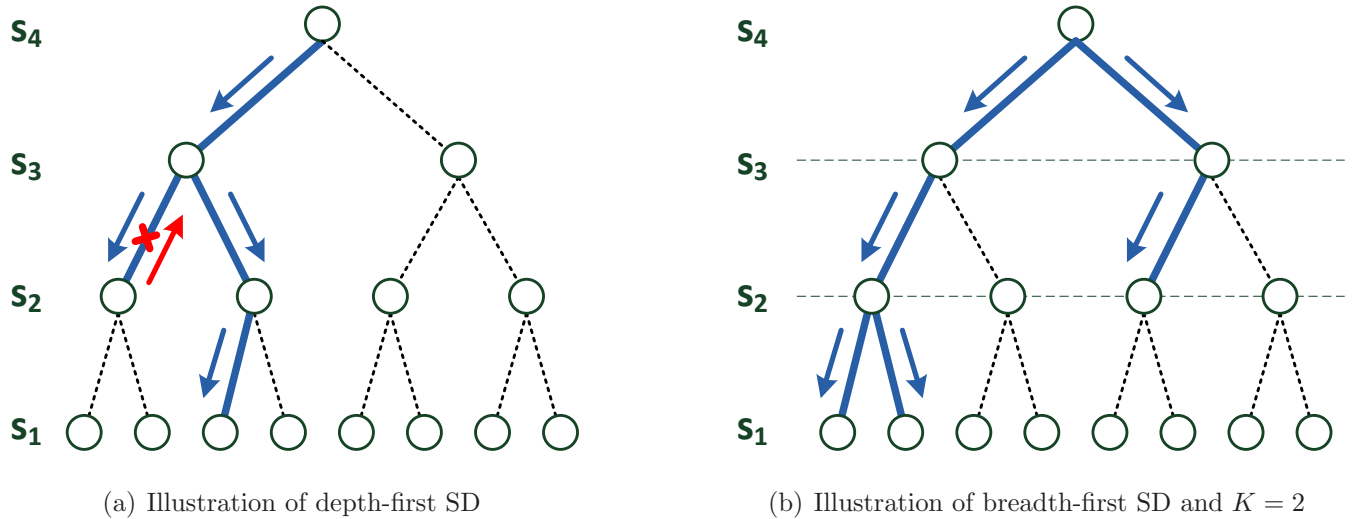
Figure 2.4: Description of depth-first and breadth-first sphere decoding

Fig. 2.4 depicts the difference of depth-first and breadth-first SD. For a 2×2 MIMO system with BPSK, depth-first search has chances to move back when the PED dissatisfy the radius constraint. However, K-Best algorithm selects 2 partial paths in each layer and only goes down while starts the searching strategy.

Obviously, the computation complexity of K-Best algorithm depends on the selection of K. In addition, the complexity is dominated by sorting K-Best PEDs at each layer. However, the performance loss is substantial if K is small and complexity is increasing with larger K. Therefore, there are lots of discussions to trade-off between the computation complexity and performance [13], [14]. Table 2.1 summerizes some characters of depth-first and breadth-first searches.

Table 2.1: Comparisom of depth-first and breadth-first sphere decoding

	Throughput	Latency	Performance
Depth-First SD	variable	Long	ML
Breadth-First SD	constant	Short	Near-ML

11

Chapter 3

Soft-output MIMO System

The additional coding gain allows the system work better when the MIMO system is combined with channel coding. Many advanced channel coding schemes, such as turbo codes [15] or low density parity check codes [16], [17], require the received data to have probabilistic information as soft value inputs instead of hard-decision inputs. In the previous chapter, the outputs of introduced algorithm are hard-decision outputs. Therefore, there are some revisions that should be applied on the algorithms.

A *list sphere decoder* (LSD) [4], which is modified from a sphere decoder, performs almost the same operations but generates different output format [18]. Not only the best guess of ML solution, a candidate list containing other symbols which have high probabilities of being ML solution is also delivered for computing the probabilistic information.

In the following sections, derivation of soft values from a list sphere decoder will be introduced first. Then the algorithms are addressed to deal with the soft output of MIMO system and the low-complexity technique will be proposed.

3.1   List Sphere Decoding Algorithm

A *list sphere decoding* (LSD) is mainly comprised of *candidate list generation* and *soft value generation*. $\mathcal{L}$, the candidate list, could be produced by the sphere decoding algorithms that mentioned in Chapter 2. And Fig. 3.1 exemplifies the realization of LSD.
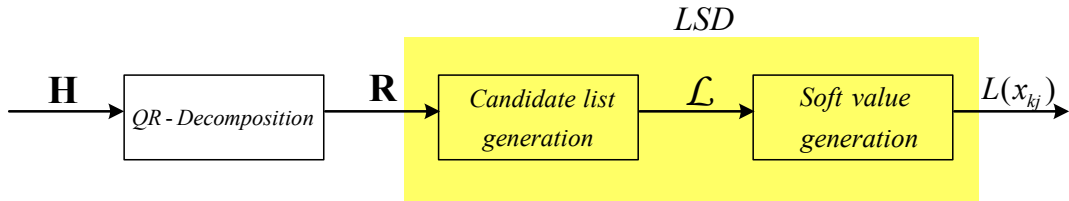
Figure 3.1: Soft-output MIMO detector

3.1.1 Decoding Algorithm

The outputs of LSD are soft values that differ from the SD. The candidate list can be generated by lots of methods. For depth-first SD, the radius is fixed until the survival paths are exceed the size of candidate list, which is $|\mathcal{L}|$. When $\mathcal{L}$ is full, the radius shrinks to the largest PED in the list. Sorting the maximum PED and radius-updating strategy is carrying out whenever adding a new path. For breadth-first search, the K-Best survival paths are the candidates in the candidate list $\mathcal{L}$. Then, the probabilistic information is generated by these candudate list.

For a binary data, log likelihood ratio (LLR) is one of the most common description of the probabilistic information for the received data. The LLR of the bit $x_{k,j}$ is defined by its a posteriori probabilities, which is

$$
\begin{aligned}
L(x_{k,j}) &= log\frac{Pr(x_{k,j}=0|\mathbf{y})}{Pr(x_{k,j}=1|\mathbf{y})} \\
&= log\frac{Pr(x_{k,j}=0)}{Pr(x_{k,j}=1)} + log\frac{Pr(\mathbf{y}|x_{k,j}=0)}{Pr(\mathbf{y}|x_{k,j}=1)},
\end{aligned}
\tag{3.1}
$$

where $x_{k,j}$ means the k-th bit mapped from the j-th symbol. Supposed $map(\cdot)$ is the M_c-PAM mapping function such that $s_k = map(x_{k,1}, x_{k,2}, \ldots, x_{k,M_c})$. The first term in (3.1) is the priori information and this term is zero for ML detection. With Gaussian noise assumption, LLR becomes

$$
\begin{aligned}
log\frac{Pr(\mathbf{y}|x_{k,j}=0)}{Pr(\mathbf{y}|x_{k,j}=1)} &= log\frac{\sum_{\mathbf{s}\in\Omega_{j,0}} Pr(\mathbf{y}|\mathbf{s})}{\sum_{\mathbf{s}\in\Omega_{j,1}} Pr(\mathbf{y}|\mathbf{s})} \\
&\approx \frac{1}{2\sigma^2}(\min_{\mathbf{s}\in\Omega_{j,1}} \|\mathbf{y}-\mathbf{Hs}\|^2 - \min_{\mathbf{s}\in\Omega_{j,0}} \|\mathbf{y}-\mathbf{Hs}\|^2) \\
&\approx \frac{1}{2\sigma^2}(\min_{\mathbf{s}\in\Omega_{j,1}\cap\mathcal{L}} \|\mathbf{y}-\mathbf{Hs}\|^2 - \min_{\mathbf{s}\in\Omega_{j,0}\cap\mathcal{L}} \|\mathbf{y}-\mathbf{Hs}\|^2),
\end{aligned}
\tag{3.2}
$$

13

where σ^2 is the noise varience, and $\Omega_{j,b}$ is the set of all $\mathbf{s}$ having $x_{k,j} = b$ for $b = 0, 1$. When QR-decomposition is performed,

$$L(x_{k,j}) = \frac{1}{2\sigma^2}\big(\min_{\mathbf{s}\in\Omega_{j,1}\cap\mathcal{L}} \|\hat{\mathbf{y}} - \mathbf{R}\mathbf{s}\|^2 - \min_{\mathbf{s}\in\Omega_{j,0}\cap\mathcal{L}} \|\hat{\mathbf{y}} - \mathbf{R}\mathbf{s}\|^2\big). \tag{3.3}$$

From (3.2), the searching range of minimum of $\mathbf{s}$ is narrowed from $\Omega_{j,1}$ to $\Omega_{j,1} \cap \mathcal{L}$. Although the complexity is reduced, the empty-set issue is occurred and will be discussed in the following.

3.1.2 Empty-set Issue

From (3.3), there are chances to encounter the situation of $\Omega_{j,1}\cap\mathcal{L} = \emptyset$ or $\Omega_{j,0}\cap\mathcal{L} = \emptyset$, which is refereed to the empty-set issue. If the problem is occurred, we could not find the minimum in the empty-set.

(a) Without the empty-set, $\Omega_{j,0}\cap\mathcal{L} \neq \emptyset$ and $\Omega_{j,1} \cap \mathcal{L} \neq \emptyset$.

(b) With the empty-set, $\Omega_{j,0} \cap \mathcal{L} = \emptyset$ and $\Omega_{j,1} \cap \mathcal{L} \neq \emptyset$.
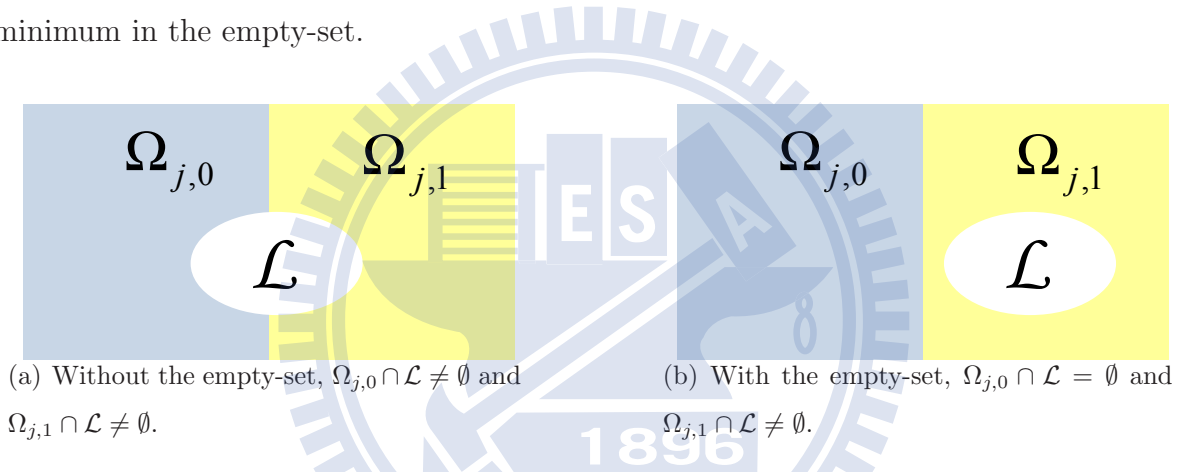
Figure 3.2: Description of the empty-set issue

As the illustration of Fig. 3.2, the minimum could be found in the Fig. 3.2(a) while Fig. 3.2(b) shows that $\Omega_{j,0}\cap\mathcal{L}$ is an empty-set. Therefore, we could try to enlarge the size of $\mathcal{L}$ until $\mathcal{L}$ includes the probability 0 of $x_{k,j}$ as the illustration of Fig. 3.3. However, the expansion has to be performed on every $x_{k,j}$ and the complexity is increasing exponentially.

On the other way, the elements from Fig. 3.2(b), the elements in the candidate list of $x_{k,j}$ are all 1 and it suggests that the probability of 1 is higher than 0. Then the subtrahend in the (3.3) could be set to a larger value which represents the larger cost. Besides, there are several other algorithms to dealing with the problem and will be introduced in the following section.
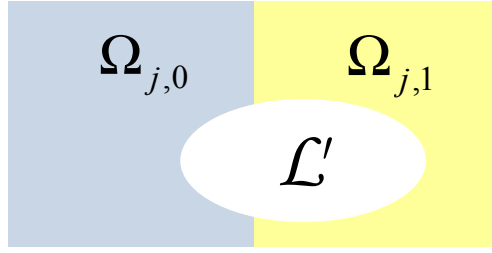
Figure 3.3: Solution to the empty-set

3.2 QOC Decoding Algorithm

QOC is an abbreviation of *OR ordered successive interference cancellation (OSIC) with candidates* [19]. The concept of this algorithm is trying to avoid the occurrence of the empty-set and narrow the size of the candidate list as small as possible. Assume the system model in Chapter 2 is applied and parameter M is referred to the number of survival paths which is similar as the parameter K in the K-Best SD. QOC decoding algorithm consists of the following four steps.

- **Step 1**- *Ordering and QR Decomposition of the Channel Matrix* $\mathbf{H}$:

  By using the methods in [20], order the channel matrix $\mathbf{H}$ and then apply QR decomposition of the channel matrix $\mathbf{H}$. Then the ML solution in (2.8) becomes

$$
\begin{aligned}
\hat{\mathbf{s}}_{ML} &= \arg \min_{\mathbf{s} \in \mathbf{\Omega}^{2N_t}} \|\hat{\mathbf{y}} - \mathbf{R}\mathbf{s}\|^2 \\
&= \arg \min_{\mathbf{s} \in \mathbf{\Omega}^{N_T}} \sum_{i=1}^{2N_T} \left(\hat{y}_i - \sum_{j=i}^{2N_T} R_{ij} s_j^{(i)} \right)^2 ,
\end{aligned}
\tag{3.4}
$$

  where $\hat{\mathbf{y}} = \mathbf{Q}^T \mathbf{y}$.

- **Step 2** - $M \times |\Omega|$ *Temporary Vector Generation*:

  This algorithm is composed of N_T stages, where each stage generates $M \times |\Omega|$ temporary vectors and selects M candidate vectors. It makes use of the M candidate vectors from the previous stage and generate $M \times |\Omega|$ temporary vectors. At stage n, each temporary vectors from $i = 2N_T - n$ to $i = 1$ is calculated by

$$
\hat{\mathbf{s}}_i = Q \left(\frac{\hat{y}_i - \sum_{j=i+1}^{2N_T} R_{ij} s_j^{(i)}}{R_{ii}} \right) ,
\tag{3.5}
$$

where $Q(\cdot)$ represents a slicing function.

- **Step 3** - *ML Metric Computation*:

  For each temporary vector obtained in Step 2, the following ML metic is determined by

  $$ML\left(\left[s_1^{(i)} s_{i+1}^{(i)} \cdots s_{2N_T}^{(i)}\right]^T\right) = \sum_{i=1}^{2N_T} \left(\hat{y}_i - \sum_{j=i}^{2N_T} R_{ij} s_j^{(i)}\right)^2, \qquad (3.6)$$

  while PED metric from (2.12) is

  $$PED\left(\left[s_n^{(i)} s_{i+1}^{(i)} \cdots s_{2N_T}^{(i)}\right]^T\right) = \sum_{i=n}^{2N_T} \left(\hat{y}_i - \sum_{j=i}^{2N_T} R_{ij} s_j^{(i)}\right)^2. \qquad (3.7)$$

  The calculation of ML metric requires more computation complexity but it avoids the empty-set issue.

- **Step 4** - *M Candidate Vector Selection and Truncation*:

  By Step 3, M candidate vectors with the smallest ML metric values are selected. And the length of the candidate vectors is reduced from N_T to n. Then Step 2 to Step 4 are repeated for each stage until the final stage 1.

A simple example is given in the Fig. 3.4. Consider a 2×2 MIMO system with $M = 1$. At stage 1 of Fig. 3.4(a), all $|\Omega|$ symbols are tried for s_4 and the remaining symbol s_3, s_2 and s_1 are generated by (3.5), which are $|\Omega|$ temporary vectors $[s_4, s_3, s_2, s_1]$. Then choose $M = 1$ survival path with the smallest ML metric by (3.6) and truncate the survival path to the partial path $[s_4]$. At stage 2 of Fig. 3.4(b), all $|\Omega|$ symbols are tried for s_3 and then for each $[s_4, s_3]$, the remaining s_2 and s_1 are also generated by (3.6). By the similar way, the procedure is iteratively performed until stage 1.

If apply QOC method in the hard decision, the QOC solution is determined by the smallest path at stage 1, such as K-Best SD. For soft output of QOC decoding, LLR calculation could be done at Step 3 and there is no chance to run into an empty-set problem. Since all $M \times |\Omega|$ temporary vector are expanded at step 2 and $\Omega_{j,0}$ or $\Omega_{j,1}$ couldn't be an empty collection. Furthermore, the calculations of ML metric (3.6) could be reused in the LLR (3.3). Thus, QOC method actually deals with the empty-set issue.

To sum up, the whole picture of hard QOC decoding method is similar as K-Best sphere decoding and soft QOC decoding method is similar as list sphere decoding. They only differ from the ordering of channel matrix and the calculations of the path metric.
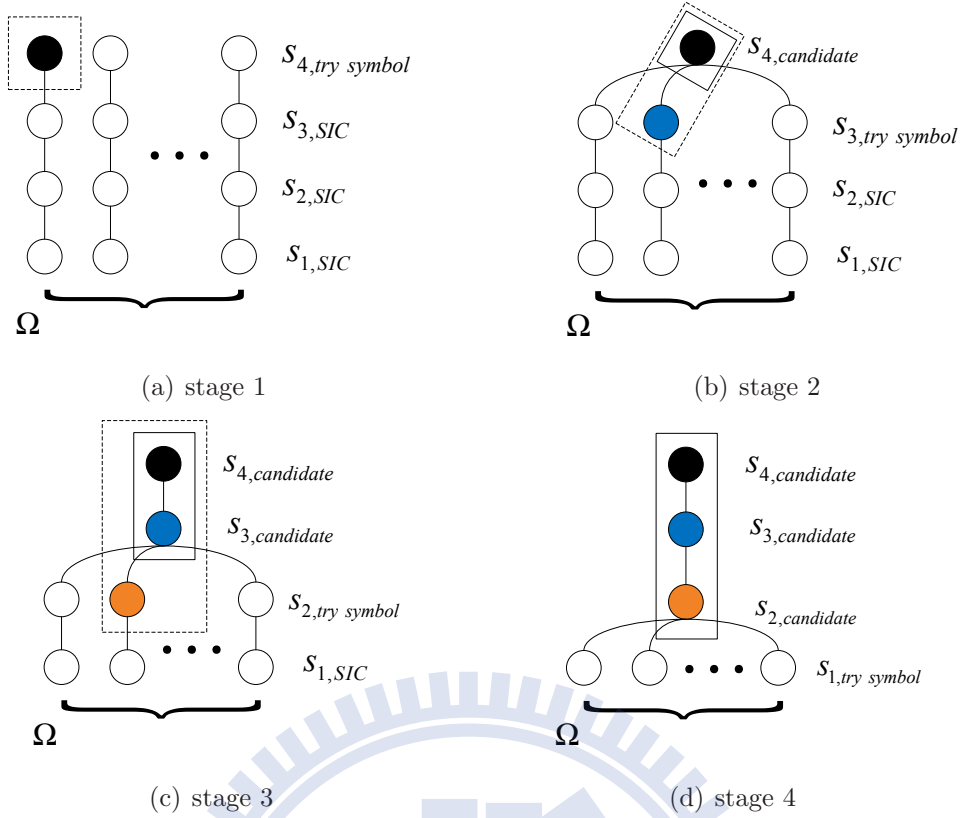
(a) stage 1 (b) stage 2

(c) stage 3 (d) stage 4

Figure 3.4: Illustration of QOC algorithm with $M = 1$ for 2×2 MIMO system.

3.3 Approach-I: Bi-Direction Decoding

Although the QOC method solves the problem of the empty-set issue, the complexity is much higher than the list sphere decoding for the same list size. Since QOC method needs to compute ML metric, the whole path $[s_{2N_T}, s_{2N_T-1}, \ldots, s_1]$ has to be calculated. In addition, the complexity is increasing dramatically especially when the modulation order Ω, the number of antenna N_T and the size of the QOC list M are increasing.

For the above reason, proposed bi-direction method comes up with a solution to reduce the complexity. The main idea is using two times of QR decomposition to reduce the calculations of ML metric. Proposed bi-direction decoding algorithm consists of the following four steps.

- **Step 1**- *QR Decomposition of the Channel Matrix* **H** *two times:*
  Same as the QOC method, channel matrix **H** is applied by the QR decomposition. Then $\mathbf{H} = \mathbf{Q_1 R_1}$ and obtain the order of symbol **s**, which is $\mathbf{\Pi_1}$. $\mathbf{\Pi_1}$ is referred as the order of channel matrix, that is, the order of the symbol to be expanded in

17

the decoding procedure. Without the loss of generality, assume the order of $\mathbf{\Pi_1}$ is $[2N_T, 2N_T - 1, \ldots, 1]$ which means that the decoding starts from s_{2N_T}, then s_{2N_T-1}, and so on. On the other hand, define $\mathbf{\Pi_2}$ as $[N_T, N_T - 1, \ldots, 1, 2N_T, 2N_T - 1, \ldots, N_T + 1]$. Then decompose $\mathbf{H}$ again by the order $\mathbf{\Pi_2}$ and $\mathbf{H} = \mathbf{Q_2}\mathbf{R_2}$.

- **Step 2** - $M \times |\Omega|$ *Temporary Vector Generation*:

  First, define a parameter P_s here, which means the degree of the applying of bi-direction. For instance, bi-direction method is performed from stage $2N_T/2$ to 1 if $P_s = 2N_T/2$. It makes use of the M candidate vectors from the previous stage and generate $M \times |\Omega|$ temporary vectors. However, at stage n and $n > P_s$, each temporary vectors from $i = N_T - n$ to $i = P_s + 1$ of first direction is calculated by

  $$\hat{\mathbf{s}}_i = Q\left(\frac{\hat{y}_i^{(1)} - \sum_{j=i+1}^{2N_T} R_{ij}^{(1)} s_j^{(i)}}{R_{ii}^{(1)}}\right). \tag{3.8}$$

  where $Q(\cdot)$ represents a slicing function, $\hat{\mathbf{y}}^1 = \mathbf{Q}_1^T\mathbf{y}$

  From second direction, temporary vectors from $i = 1$ to $i = P_s$ is

  $$\hat{\mathbf{s}}_i = Q\left(\frac{\hat{y}_{2N_T+1-i}^{(2)} - \sum_{j=2N_T+2-i}^{2N_T} R_{(2N_T+1-i)j}^{(2)} s_j^{(i)}}{R_{(2N_T+1-i)(2N_T+1-i)}^{(2)}}\right), \tag{3.9}$$

  where $\hat{\mathbf{y}}^2 = \mathbf{Q}_2^T\mathbf{y}$.

  If at stage $n \le P_s$, each temporary vectors from $i = 1$ to $i = n - P_s$ of second direction is calculated by

  $$\hat{\mathbf{s}}_i = Q\left(\frac{\hat{y}_{2N_T+1-i}^{(2)} - \sum_{j=2N_T+2-i}^{2N_T} R_{(2N_T+1-i)j}^{(2)} s_j^{(i)}}{R_{(2N_T+1-i)(2N_T+1-i)}^{(2)}}\right). \tag{3.10}$$

- **Step 3** - *ML Metric Computation*:

  For each temporary vector obtained in Step 2, the following *bi-direction metic* (BM) is determined by $BM\left([s_1 s_{i+1} \cdots s_{2N_T}]^T\right)$. And if at stage n and $n > P_s$,

  $$\begin{aligned} BM\left(\left[s_1^{(i)} s_{i+1}^{(i)} \cdots s_{2N_T}^{(i)}\right]^T\right) &= \sum_{i=P_s+1}^{2N_T} \left(\hat{y}_i^{(1)} - \sum_{j=i}^{2N_T} R_{ij}^{(1)} s_j^{(i)}\right)^2 \\ &+ \sum_{i=1}^{P_s} \left(\hat{y}_{2N_T-i+1}^{(2)} - \sum_{j=i}^{2N_T-i+1} R_{(2N_T-i+1)j}^{(2)} s_j^{(i)}\right)^2 \end{aligned} \tag{3.11}$$

18

On the other hand, if at stage n and $n \leq P_s$,

$$
\begin{aligned}
BM\left(\left[s_1^{(i)} s_{i+1}^{(i)} \cdots s_{2N_T}^{(i)}\right]^T\right) &= \sum_{i=n-P_s+1}^{2N_T}\left(\hat{y}_i^{(1)} - \sum_{j=i}^{2N_T} R_{ij}^{(1)} s_j^{(i)}\right)^2 \\
&+ \sum_{i=1}^{n-P_s}\left(\hat{y}_{2N_T-i+1}^{(2)} - \sum_{j=i}^{2N_T-i+1} R_{(2N_T-i+1)j}^{(2)} s_j^{(i)}\right)^2 (3.12)
\end{aligned}
$$

- **Step 4** - *M Candidate Vector Selection and Truncation*:

  This step is almost the same as QOC method. By Step 3, M candidate vectors with the smallest ML metric values are selected. And the length of the candidate vectors is reduced from N_T to n. Then Step 2 to Step 4 are repeated for each stage until the final stage 1.
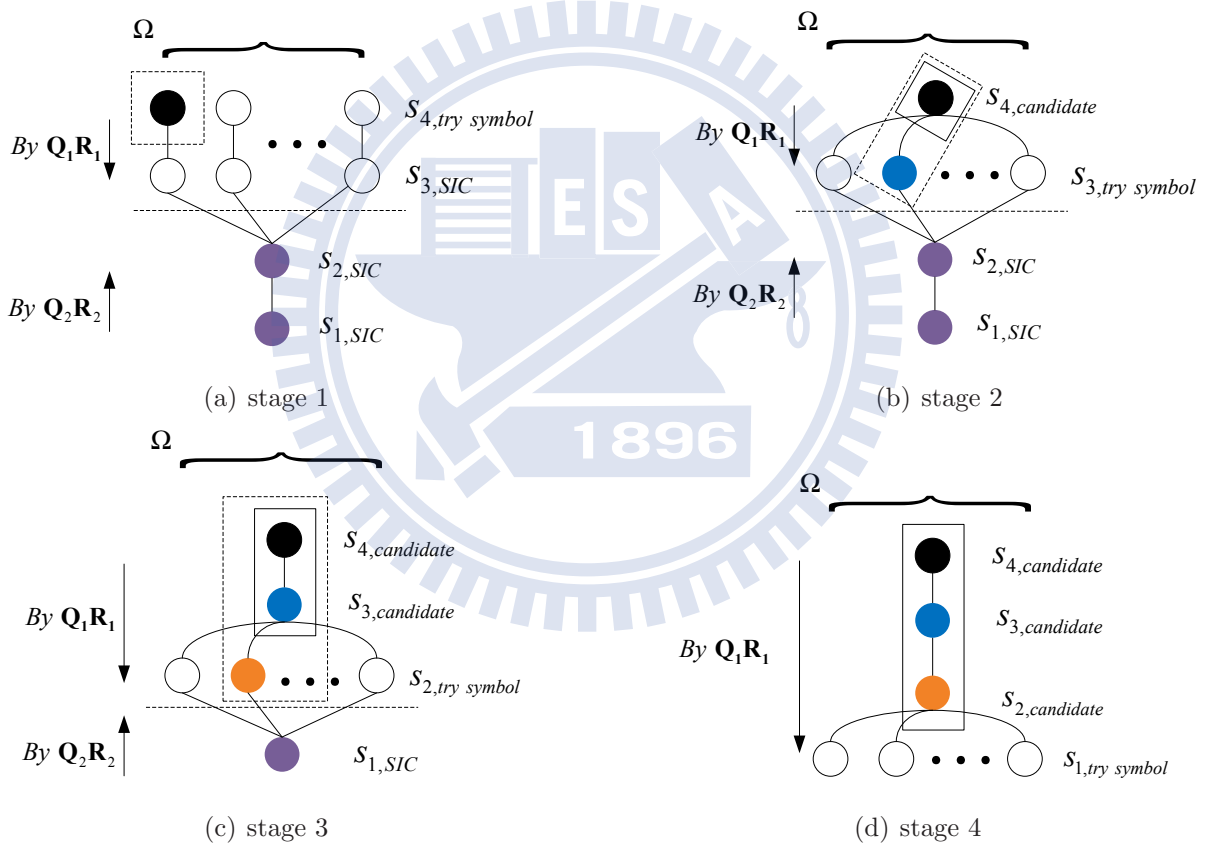
Figure 3.5: Illustration of bi-direction algorithm with $M = 1$ and $P_s = 4$ for 2×2 MIMO system.

A simple illustration is depicted in Fig. 3.5. Also consider a 2×2 MIMO system with $M = 1$ and $P_s = 2N_T/2 = 2$ as an example. At stage 1 of Fig. 3.5(a), all $|\Omega|$ symbols are

tried for s_4 and the remaining symbol s_3, s_2 and s_1 are generated by (3.8), which are $|\Omega|$ temporary vectors $[s_4, s_3, s_2, s_1]$. In addition, s_4 and s_3 are calculated by $\mathbf{Q_1 R_1}$, while s_2 and s_1 are computed by $\mathbf{Q_2 R_2}$. Furthermore, s_2 and s_1 could be calculated only once, the same values are applied at the rest of stages. Then choose $M = 1$ survival path with the smallest ML metric by (3.9) and truncate the survival path to the partial path $[s_4]$.

At stage 2 of Fig. 3.5(b), all $|\Omega|$ symbols are tried for s_3 which is calculated by $\mathbf{Q_1 R_1}$ and then for each $[s_4, s_3]$, the remaining s_2 and s_1 are the values computed at sate 1. Then choose $M = 1$ survival path with the smallest ML metric by (3.9) and truncate the survival path to the partial path $[s_4, s_3]$.

From stage 3 ($3 > P_s = 2$) of Fig. 3.5(c), all $|\Omega|$ symbols are tried for s_2 which is calculated by $\mathbf{Q_1 R_1}$ and then for each $[s_4, s_3, s_2]$, the remaining s_1 is the value computed at sate 1 which is calculated by $\mathbf{Q_2 R_2}$. That is, bi direction method is applied only from symbol s_{P_s-1} to s_1 when number of stage is larger then P_s. Then choose $M = 1$ survival path with the smallest ML metric by (3.9) as well and truncate the survival path to the partial path $[s_4, s_3, s_2]$. In the leaf node of s_1, the same operations are performed as QOC decoding in Fig. 3.5(d).

In a word, bi-direction method disperses the calculations by $\mathbf{Q_1 R_1}$ and $\mathbf{Q_2 R_2}$. From $i = 2N_T - n$ to $i = 1$ where n is referred to stage, QOC method has to calculate the remaining symbol by (3.5). However, bi-direction method takes advantage of the characters of upper triangular matrix $\mathbf{R_1}$ and $\mathbf{R_2}$ to reduce the computation of complexity.

Figure 3.6: Matrix illustration of bi-direction.

20

From Fig. 3.6, the calculation of (3.5) is increasing from the root node, layer $2N_T$, to the leaf node, layer 1. Bi-direction method replaces the upper part of original $\mathbf{R}$ with the lower part of $\mathbf{R_2}$. Therefore, this method could reduce the complexity in the decoding procedure. And the complexity analysis is given at the following section.

3.4   Complexity Analysis

The complexity of three different soft-ouput MIMO decoder is given in Table 3.1. The computation complexity compares in terms of multiplications. And divisions have to be applied on bi-direction and QOC method. Thus, the factor C is used to represent a multiple of the hardware complexity between divisions and multiplications.

From the table, the multiplication operations of bi-direction at QR decomposition are 2 times of QOC and LSD. However, the multiplications of bi-direction at LLR caculation are much less than QOC and LSD for the same list size. In addition, the sorting comparison depend on the list size, K or M. Furthermore, parameter P_s of bi-direction is another tradeoff between complexity and performane. If bi-direction performed at more stages, the complexity is lower while the performance loss is greater. Therefore, a designer could choose a proper parameter to meet the desired spec at the lowest cost.

Table 3.1: Comparisom of three soft-output MIMO decoders.

	Multiplications at LLR Calculation	Multiplications at QR Decomposition	Sorting Comparison
Bi-direction	$\Omega[\sum_{i=1}^{P_s} i + P_s(C+2) - C$ $+M[\sum_{j=1}^{P_s-2}\sum_{i=j+1}^{P_s-1} i$ $+(2+C)\sum_{i=1}^{P_s-2} i$ $+(P_s-2)(C+2)P_s - C]$ $+\sum_{i=1}^{N_T-P_s-1} i + (2N_T - P_s)(c+2)]$	$2(C+1)(2N_T)^2$ $+2CN_T$ $+2(2N_T+1)\sum_{i=1}^{2N_T-1} i$	$\Omega[M(2N_T-2)$ $+\Omega+1]$
QOC	$\Omega[\sum_{i=1}^{2N_T-1} i + C(2N_T - 1)$ $+M(\sum_{i=2}^{2N_T-1}\sum_{i=j}^{2N_T-1} i$ $+(2+C)\sum_{i=1}^{2N_T-2} i)]$	$(C+1)(2N_T)^2$ $+CN_T$ $+(2N_T+1)\sum_{i=1}^{2N_T-1} i$	$\Omega[M(2N_T-2)$ $+\Omega+1]$
LSD	$\Omega[|\mathcal{L}|\sum_{i=1}^{2N_T-2}(i+3)$ $+2+3\Omega]$	$(C+1)(2N_T)^2 + CN_T$ $+(2N_T+1)\sum_{i=1}^{2N_T-1} i$	$\Omega[|\mathcal{L}|(2N_T-2)$ $+\Omega+1]$

Chapter 4

LDPC-Coded MIMO System

In Chapter 3, list sphere decoding algorithm and other decoding method have been shown to be an efficient and applicable approach to realize ML detection for MIMO systems. Combined with channel coding scheme, the additional coding gain allows the system work better in lower SNR environment. Now, many advanced communication systems such as wireless local area network (IEEE802.11n [21]), wireless metropolitan network (IEEE802.16e [22]), and 10G BASE-T Eithernet (IEEE802.3an [23]), employ *low-density parity-check* (LDPC) code as the forward error correction (FEC) technique.

In the following section, LDPC code decoder will be introduced first. Then a method of connecting MIMO detection and LDPC to improve the performance is brought up.

4.1 Low Density Parity Check Codes

In 1963, Gallager [16] first introduced and proved *low-density parity-check* (LDPC) code as a powerful error control scheme. Until the advances in VLSI technology, LDPC codes were almost forgotten in the subsequent thirty years. Rediscovered by Mackay [17] and then shown to be capacity-approaching, interests in LDPC codes eventually rose in the late 1990s. The simple arithmetic computations and implicit parallelism of the LDPC decoding algorithms facilitate low-complexity and high-speed hardware implementations.

The log-likelihood ratio (LLR) of intrinsic information of nth variable node is denoted by P_n. The message from n^{th} variable node to m^{th} check node is denoted by z_{mn}. The message from m^{th} check node to n^{th} variable node is denoted by ϵ_{mn}. The a posteriori

LLR of nth bit is denoted by z_n. The current number of iteration and maximum number of iteration is represented by i and I_{Max} respectively. The standard BP is carried out as followed.

- **Step 1 - Initialzation:**

  Set $i = 1$. For each m, n, set $z_{mn}^0 = P_n$

- **Step 2 - Iterative Decoding:**

  (a) check node to variable node update step, for $1 \le m \le M$ and each $n \in N(m)$, process

$$\epsilon_{mn}^i = 2 \tanh^{-1} \left(\prod_{n' \in N(m) \backslash n}^{d} \tanh(\frac{z_{mn'}^{i-1}}{2}) \right) \tag{4.1}$$

  (b) variable node to check node update step, for $1 \le n \le N$ and each $m \in M(n)$, process

$$z_{mn}^i = P_n + \sum_{m' \in M(n) \backslash m} \epsilon_{m'n}^i \tag{4.2}$$

$$z_n^i = P_n + \sum_{m' \in M(n)} \epsilon_{m'n}^i \tag{4.3}$$

- **Step 3 - Hard Decision:**

  Let X_n be the nth bit of decoded codeword. If $z_n^{(i)} \ge 0, X_n = 0$, else if $z_n^{(i)} < 0, X_n = 1$. If $H(x^{(i)})^t = 0$ or I_{MAX} is reached, the decoder stops and outputs the codeword. Otherwise, it sets $i = i + 1$ and goes on iterative decoding.

The iterative decoding processes for one iteration of standard BP is illustrated below. The messages are updated in parallel way between check nodes and variable nodes. The process is shown in Fig. 4.1.

As it is shown in (4.1), the nonlinear function of hypertangent is the most complicated operation in computing ϵ_{mn}^i. Therefore, min-sum alogorithm [24] is proposed to reduce the complexity. The decoding algorithm is the same as original BP algorithm and only modifies the equation of check node to bit node update. (4.1) becomes

$$\epsilon_{mn}^i \approx \left(\prod_{n' \in N(m) \backslash n}^{d} \cdot sign(z_{mn'}^{i-1}) \right) \min_{n' \in N(m) \backslash n} \left| z_{mn'}^{i-1} \right|. \tag{4.4}$$

(a) Check node to variable node update of BP algorithm

(b) Varibale node to check node update of BP algorithm

Figure 4.1: Illustratin of standard BP.

Furthermore a scaling factor β is applied to compensate the performance loss. That is, (4.4) adjusts to

$$\epsilon_{mn}^{i} \approx \left(\prod_{n' \in N(m) \backslash n}^{d} sign(z_{mn'}^{i-1}) \right) \min_{n' \in N(m) \backslash n} \cdot \left| z_{mn'}^{i-1} \right| \times \beta, \tag{4.5}$$

where $0 < \beta < 1$.

4.2   LDPC-Coded MIMO System

In this section, the whole simulation environment will be introduced first. Then the two-stage algorithm will be applied on the channel-coded MIMO receiver. In addition, simulations based on the LDPC codes defined in IEEE802.16e (WiMax) [22] are presented in the following. An LDPC-Coded 16-QAM and 64-QAM 4×4 MIMO system was simulated. Randomly generated binary data are encoded by $(2304, 1152)$ LDPC code. By direct spatial mapping, the coded information is transmitted via an uncorrelated flat fading channel which is mentioned in Chapter 2 and applied min-sum algorithm as the LDPC decoding algorithm. And the iteration of LDPC is at most 30. The whole simulation environment is illustrated in Fig. 4.2. First, an information bit stream $\mathbf{b}$ is generated randomly and encoded by LDPC. Then symbols transmit after signal and spatial mapping. When the signals detect by MIMO detection and generate the LLR values, LDPC decodes the code words into bit information.
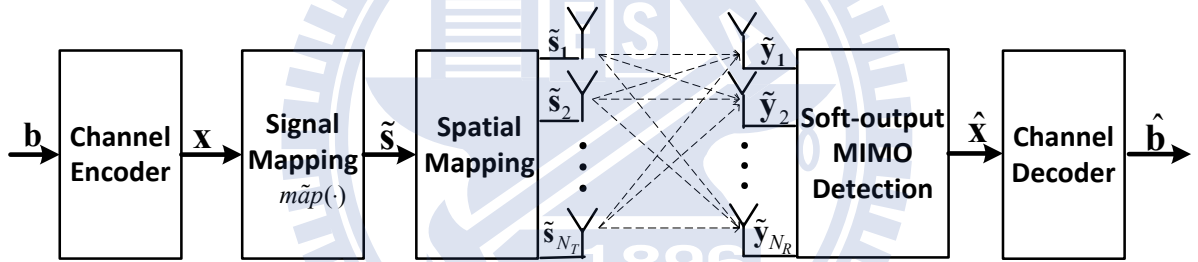
Figure 4.2: Channel-coded MIMO system

4.3 Approach-II: Nonlinear Quantization

In this section, we will propose a *nonlinear quantization* method (NLQ) to improve the performance of LSD. As mentioned at Chapter 3, a large probability value is set to the empty set if the issue occurs in LSD. That is, the first term or the second term defined in the (3.2) is fixed to a large constant, which is 10 as a simulated parameter here.

Obviously, the performance of BER highly depends on the size of list $|\mathcal{L}|$ since the empty set seldom occurs when the size of list is larger. NLQ provides a simple way to improve the performance of soft-output MIMO decoder. NLQ truncates the output LLRs of MIMO system and the inputs of LDPC decoder by a positive parameter γ. The soft-values generated by (3.2) quantized between γ and $-\gamma$ as Fig. 4.3 shown. The LLRs are truncated to γ if the values are larger than γ; the LLRs are quantized to γ while they are smaller than $-\gamma$. At Fig. 4.4, a real LLR distribution is given to show clearly.
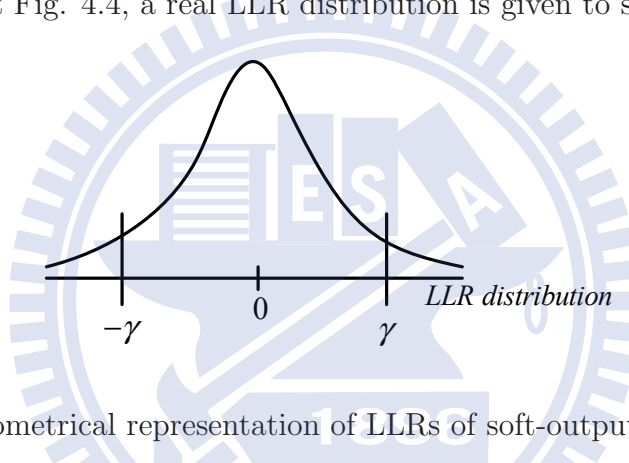
Figure 4.3: Geometrical representation of LLRs of soft-output MIMO decoder.

As the illustration of Fig. 4.4, the original LLR distribution from LSD is depicted in Fig. 4.4(a). And we perform NLQ with $\gamma = 6$ which quantizes the original LLRs between 6 and -6. The resulted LLR distribution is depicted as Fig. 5.7(b). NLQ is applied on channel-coded MIMO system befer error control code and after MIMO detection. And the simulation results will be given in the next chapter.
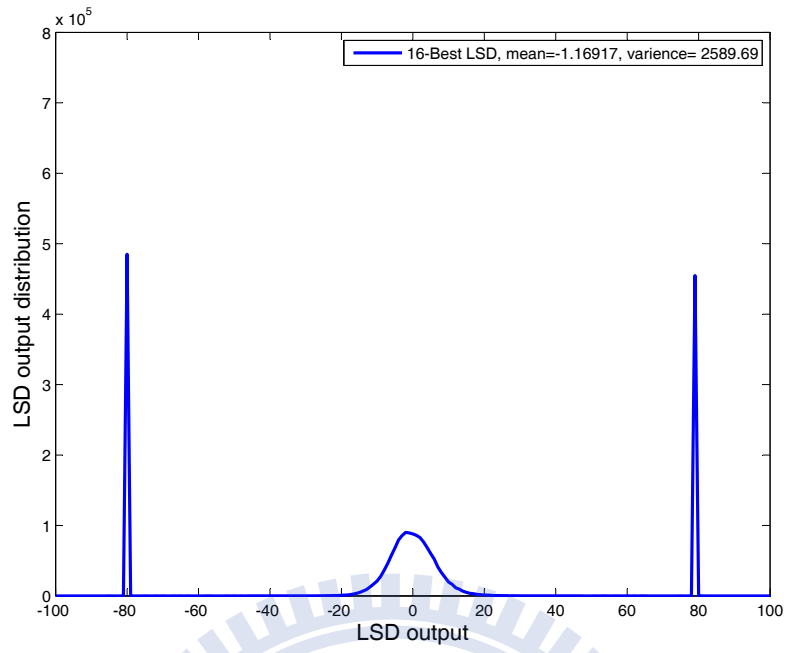
(a) LLR distribution before NLQ.
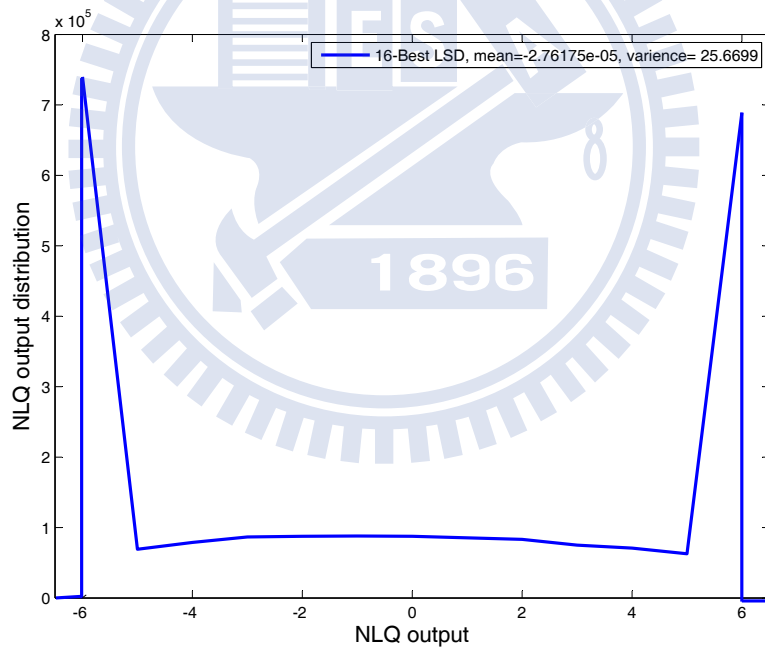
(b) LLR distribution after NLQ and $\gamma = 6$.

Figure 4.4: LLR distribution of $(2304, 1152)$ LDPC-coded 16-QAM 4×4 system at 12 dB.

4.4 Approach-III: Two-Stage Algorithm

In this section, a method to improve the bit error rate (BER) of channel-coded MIMO system is proposed. A reversed list Φ which stores some unreliable bits from MIMO detection is defined. And the flow chart of two-stage algorithm is given as Fig. 4.5.
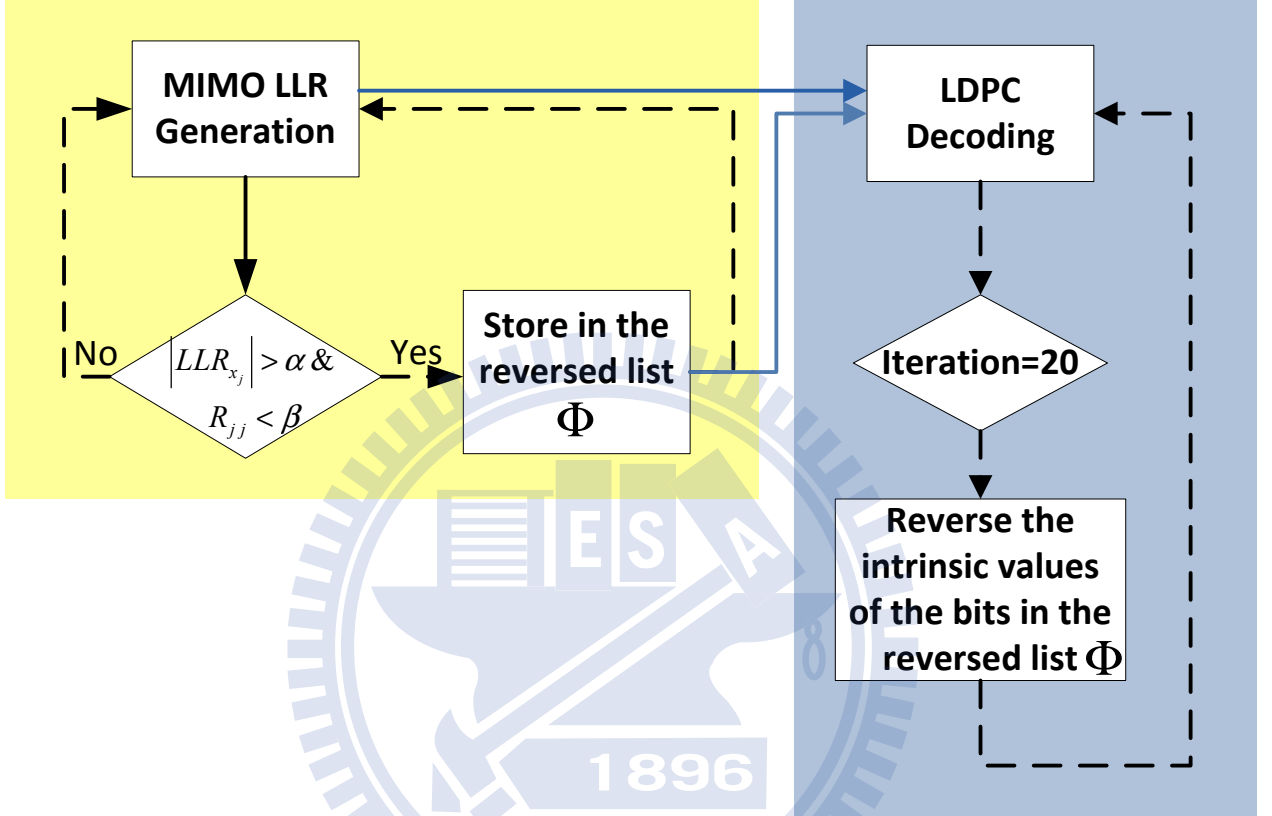

Figure 4.5: Flow chart of two-stage algorithm

First, unreliable bits are chosen from the MIMO detection. We define two positive factor α and β here. If the quantity of LLR of x_j is larger than α which means that the bit is strong at 0 or strong at 1. This infers that the channel to transmit the bit x_j is good and the channel gain of this antenna should large. And the diagonal elements of $\mathbf{R}$ is used as the measurement of the channel gain. Thus, we could assume the bit x_j is not reliable if the LLR value is larger than α and $\mathbf{R}_{jj}$ is smaller than β. After the preliminary sieving, the unreliable bit is stored in the reversed list Φ.

After a block of LDPC codeword is detected by MIMO detection, n bits in the reversed

list Φ is selected and send to the LDPC decoder and then start the LDPC decoding algorithm. At stage 1 which LDPC decodes before 20 iterations, the LLR values from MIMO detection remain unchanged. At stage 2 which LDPC decodes at 20 iterations, we flip the LLRs of bits that are in the reversed list Φ and then start the LDPC decoding procedure again. By this two-stage method, some errors could be corrected by the LDPC decoder and improve the error performance, and the performane will be shown in Chpater 5.

The complexity overhead of two-stage algorithm is that some comparsions are prformed while MIMO detection and LDPC decoding. The comparisons at MIMO detection are performed to choose the unreliable bits and then choose n bits in the reversed list Φ. Besides, flipping the bits in the reversed bit also cost some extra comparison operations. Therefore, there is another tradeoff between performance and complexity.

30
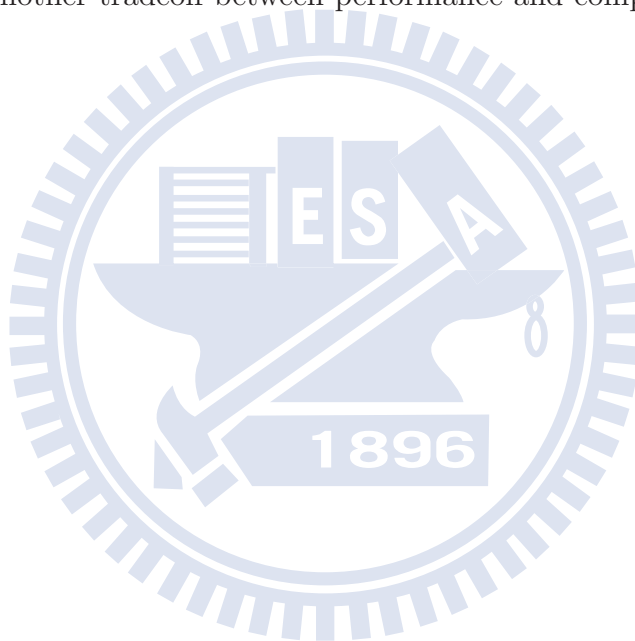
Chapter 5

Simulation Results and Comparison

In this chapter, the performance and the computation complexity trade-off between QOC and bi-direction method are given first. And the error performance of MIMO dection methods with NLQ are discussed. Then we will present the error performance of two-stage algorithm. The following discussion is shown by 16-QAM 4×4 MIMO system with $(2304, 1152)$ LDPC decoder defined in 802.16e [22] and the LDPC decoding algorithm is applied by normalized min-sum algorithm with scaling factor 0.75. In addition, the number of iteration of LDPC is 30. In the end, all proposed algorithms are summarized by 64-QAM 4×4 MIMO system with $(2304, 1152)$ LDPC decoder defined in 802.16e [22].

5.1 Bi-Direction Method

The error performance and the complexity comparison of LSD, proposed bi-direction and QOC method are given in this section. Fig. 5.1(a) shows the BER of 16-Best LSD and the QOC and bi-direction method for parameter $M = 4$. Fig. 5.1(b) shows the performance of 32-Best LSD and the QOC and bi-direction method for parameter $M = 8$. In addition, the parameter $P_s = 4$ is considered in the bi-direction method. From Fig. 5.1, the error performance of all these three algorithms improves when the size of list is expended, parameter M for bi-direction and QOC method and parameter $|\mathcal{L}|$ for LSD. In addition, bi-direction and QOC method could approach LSD with smaller M which is almost quarter of $|\mathcal{L}|$.
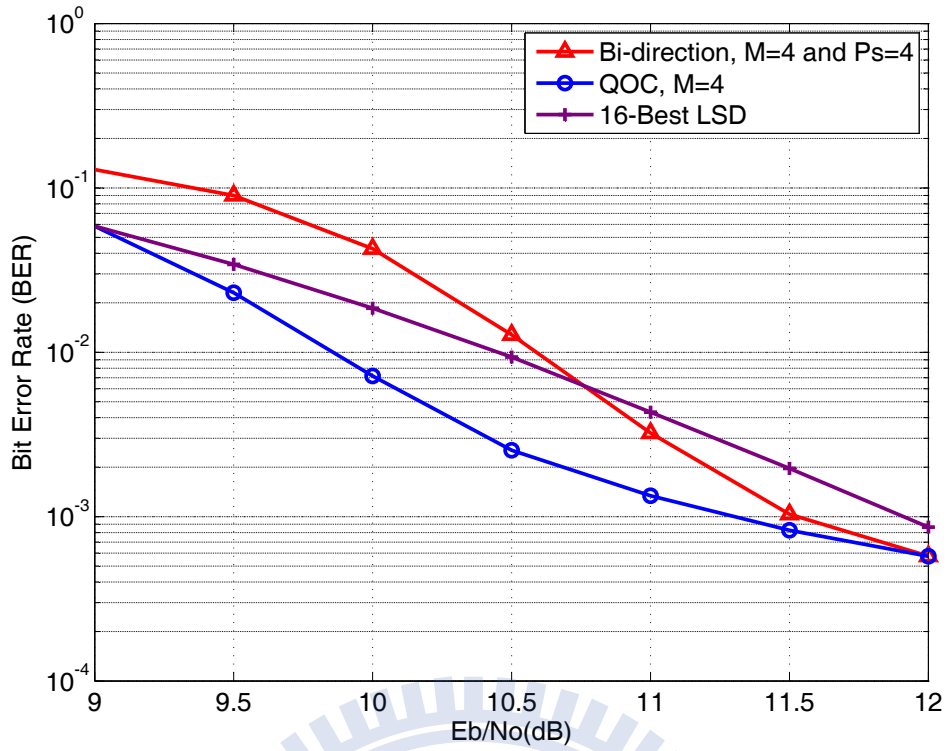
(a) $M = 4$ for bi-direction and QOC, and $|\mathcal{L}| = 16$ for LSD.
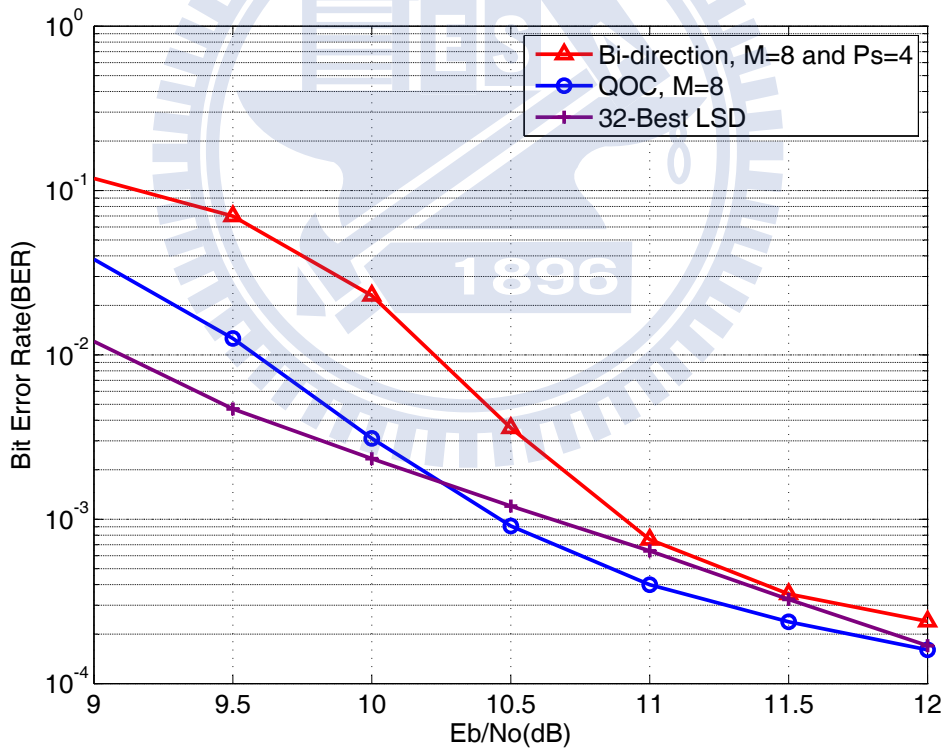
(b) $M = 8$ for bi-direction and QOC, and $|\mathcal{L}| = 32$ for LSD.

Figure 5.1: BER of $(2304, 1152)$ LDPC-coded 16-QAM 4×4 system.
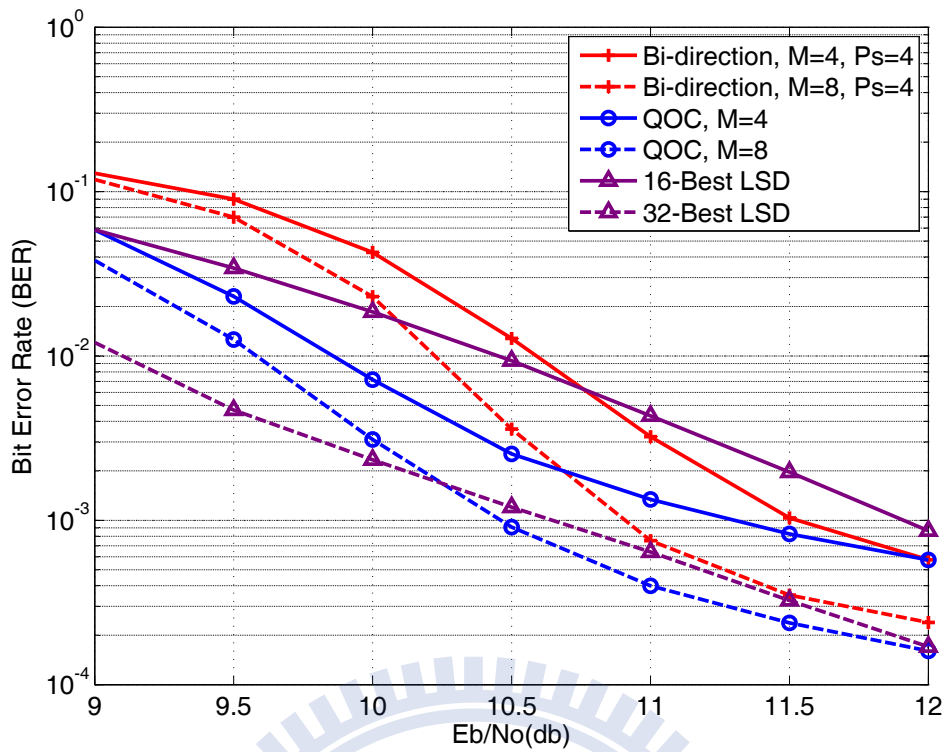
Figure 5.2: BER of $(2304, 1152)$ LDPC-coded 16-QAM 4×4 system.
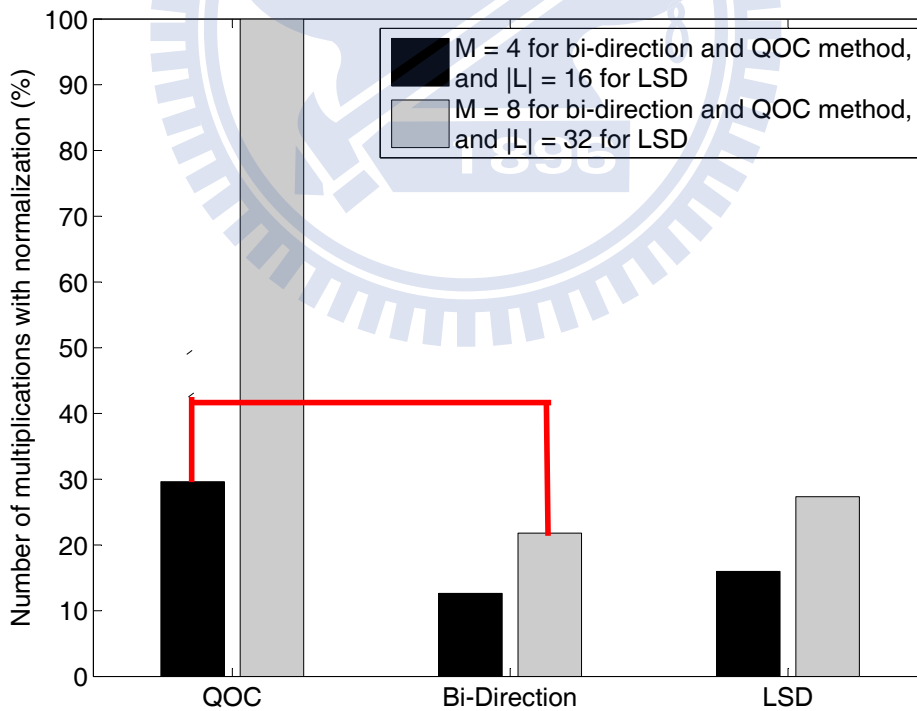
Figure 5.3: Complexity comparison of 16-QAM 4×4 system in terms of multiplications.

Figure 5.4: Illustration of complexity reduction for the similar performance at QOC $M = 4$ and bi-direction $M = 8$, $P_s = 4$.

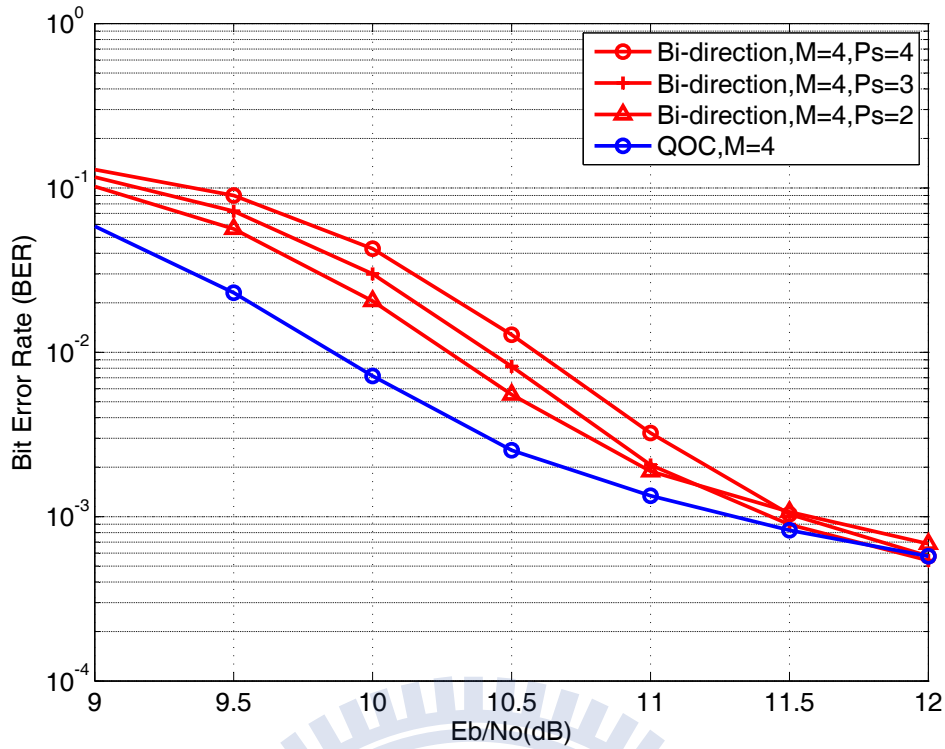Figure 5.5: BER of $(2304, 1152)$ LDPC-coded 16-QAM 4×4 system.

Although the performance loss of bi-direction from QOC at BER 10^{-3} is about 0.2 dB as $M = 4$ and 0.5 dB as $M = 8$, the complexity reduction is about 50% and 70% of QOC respectively which is shown in the Fig. 5.3. And the sorting comparison of bi-direction method also reduces to 33% of LSD. Furthermore, the complexity of bi-direction is always the lowest in these three algorithms at the similar performance. Therefore, the bi-direction method provides a way to reduce the complexity. Fig. 5.2 combines Fig. 5.1(a) and Fig. 5.1(b). The BER performance of QOC $M = 4$ is similar to bi-direction method $M = 8$ and $P_s = 4$. And Fig. 5.3 shows that the complexity of bi-direction method is only about 66% of QOC. The simpilfied illustration of computation comparison of QOC and bi-direction method is shown in Fig. 5.4. Bi-direction method calculates 9 times smaller diagonal matrices and 1 additional QR decomposition to replace 4 times full diagonal matrices calculation of QOC. For 16-QAM 4×4 system, the ratio of computation between QOC and bi-direction is about $\frac{1}{2}(8 \times 8) \times 4 : (\frac{1}{2}(4 \times 4) \times 9 + \frac{1}{2}(8 \times 8)) = 16 : 13$. Therfore, bi-direction method actually reduces the computation complexity.

In addition, the stage parameter, P_s, has impact on the BER as shown in Fig. 5.5. If

bi-direction applied on fewer stages, that is, smaller P_s, the performance loss is less while the complexity is increasing. When P_s equal to 1, the BER performance is the same as QOC method. Therefore, P_s is another tradeoff between performance and complexity.

5.2 Nonlinear Quantization

In this section, we will show the performance comparison before NLQ and after NLQ. Let us cosider different γ of NLQ method. In the Fig. 5.6(a), different γ has influence on the performane. For 16-Best LSD, if LLRs quantize at smaller γ, the varience of LLRs is too small for LDPC decoder and the information for every bits is too few to decode. Because LDPC decoding algorithm is derived by binary phase shift keying (BPSK) modulation, LDPC decoder maybe preferr a kind of input LLRs. Therefore, the performance degrades when γ exceeds 6 for 16-Best LSD which is depicted from Fig. 5.6(b). From this experiment, $\gamma = 6$ is choosen as the following simulation.

The real lines in Fig. 5.7(a) is referred to the original bit error rate of LSD with different list size and the dash lines represent the performance of NLQ method applied on LSD. From Fig. 5.7(a), the BER of LSD with NLQ will improve almost 2dB. In addition, the performance gain is established for different list size, $|\mathcal{L}|$.

Not only LSD, the NLQ method also improves the performance of bi-direction method and QOC which is given at the Fig. 5.8. The performance after NLQ improves almost 2 dB both in the QOC and bi-direction method as well.

For the different channel coding scheme, the improvement by NLQ also comes into existence. The LDPC decoder is replaced with a rate-$\frac{1}{2}$ soft Viterbi decoder at Fig. 5.9 and NLQ parameter $\gamma = 4.5$ is applied here. LSD after NLQ at BER 10^{-4} improves about 1.7 dB in 64-Best LSD.
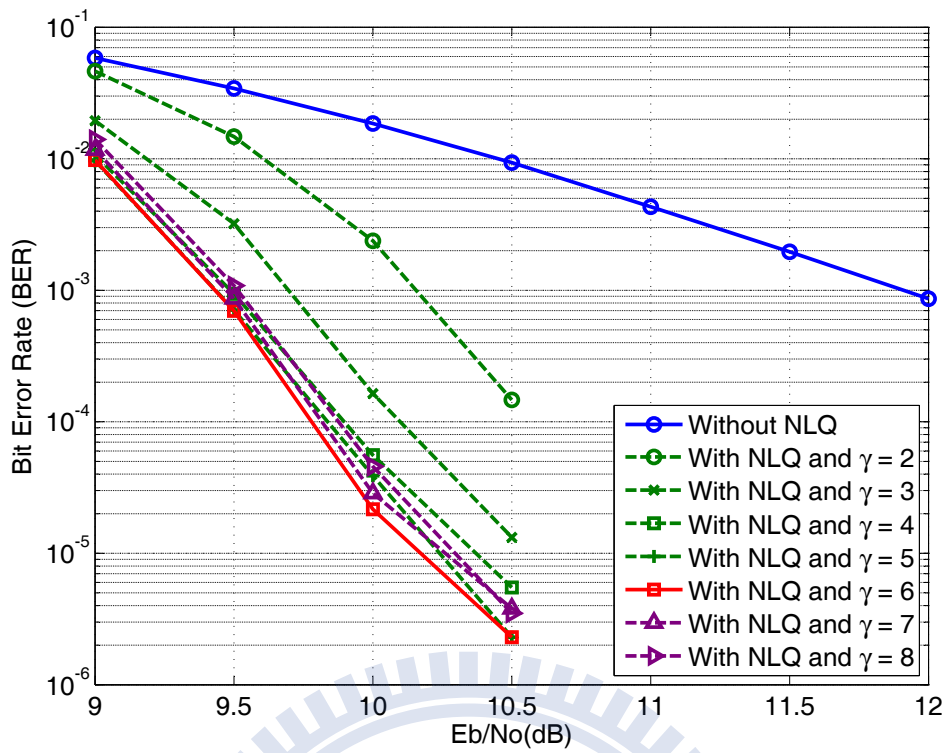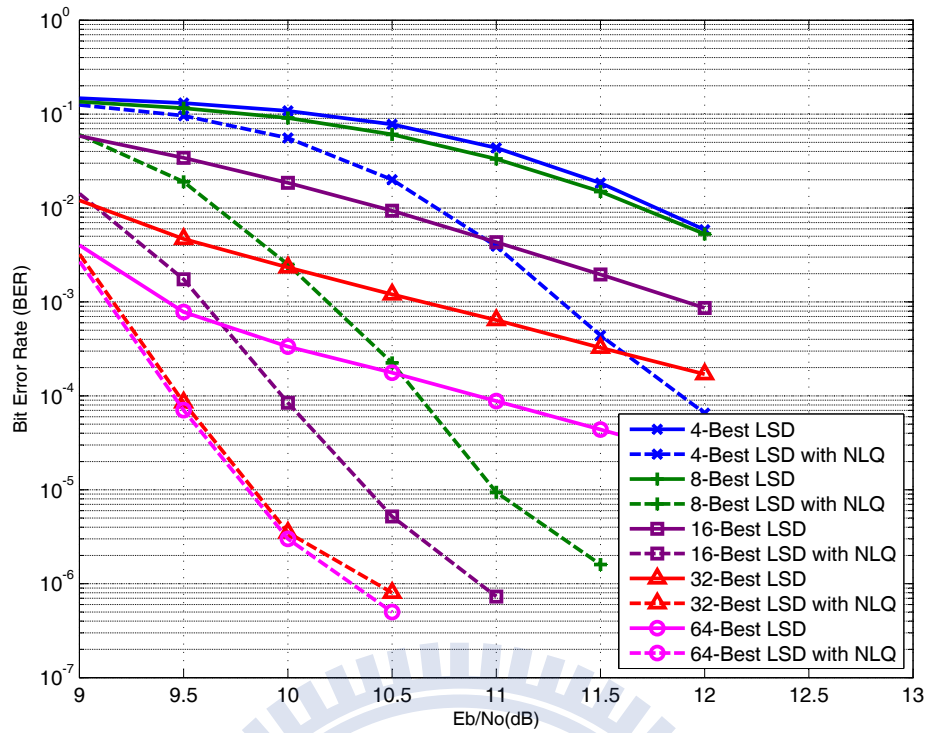
(a) 16-Best LSD after NLQ versus different γ.
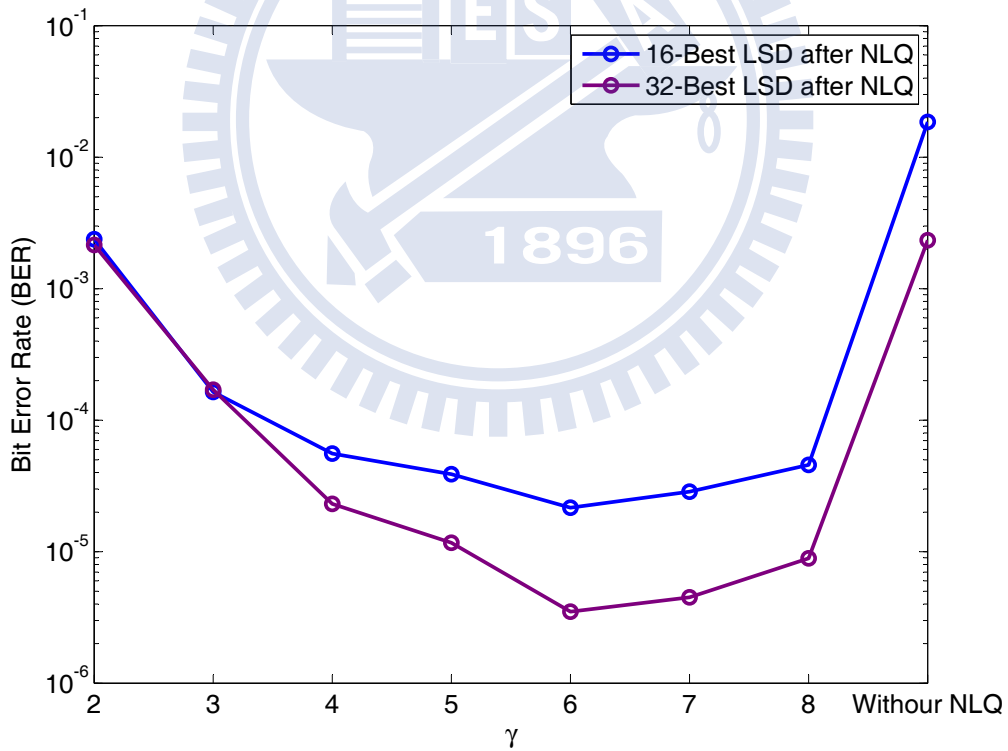
(b) At 10dB, 16-Best LSD and 32-Best LSD after NLQ versus different γ.

Figure 5.6: BER of $(2304, 1152)$ LDPC-coded 16-QAM 4×4 system versus different γ.

(a) LSD after NLQ with different list size.
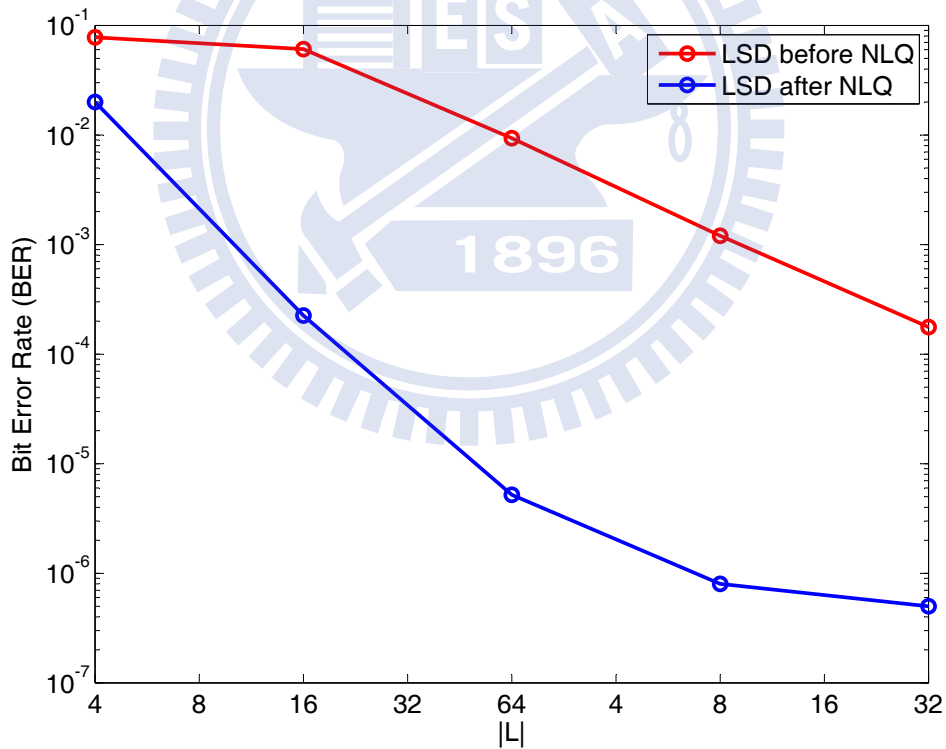
(b) At 10dB, LSD after NLQ with differen list size.

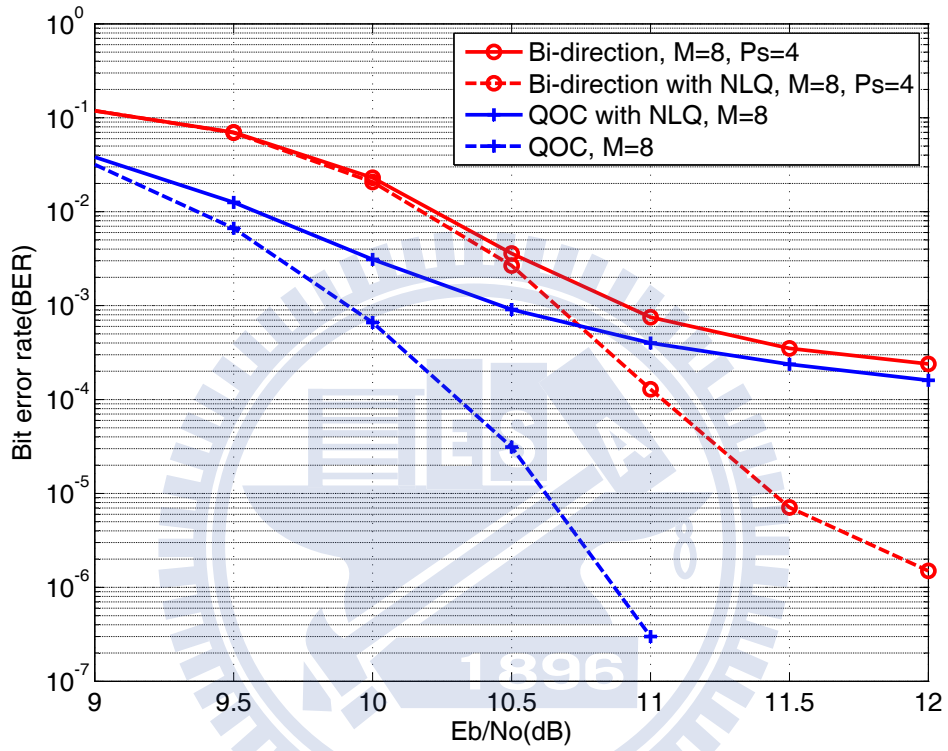Figure 5.7: BER of $(2304, 1152)$ LDPC-coded 16-QAM 4×4 system after NLQ.

Figure 5.8: BER of $(2304, 1152)$ LDPC-coded 16-QAM 4×4 system with bi-direction and QOC method, and $\gamma = 6$.
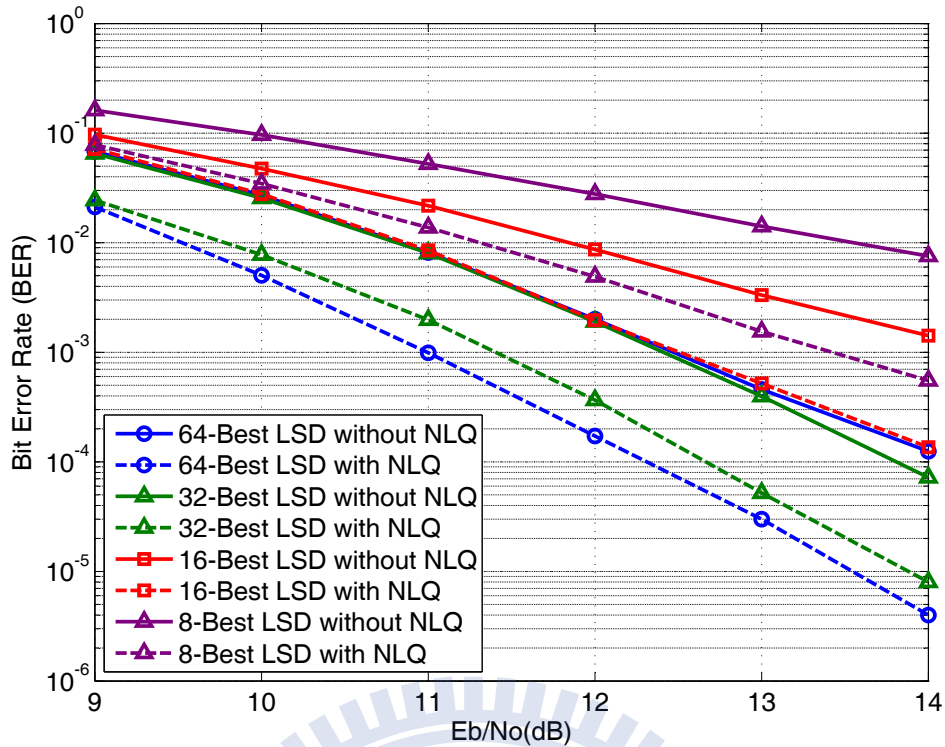
Figure 5.9: BER of rate-$\frac{1}{2}$ Viterbi-coded 16-QAM 4×4 system, and$\gamma = 4.5$.

5.3 Two-Stage Algorithm

As mentioned in Chapter 4, we perform the two-stage algorithm on the 4×4 LDPC-coded MIMO system after NLQ. A 10 bit reversed list stores the most unreliable bits from soft-output MIMO decoder. These 10 bits are determined if the LLR values are larger than 5 and the corresponded channel gain is less than 0.5. That is, the simulated parameter α is 5 and β is 0.5. After LDPC decoding performs 20 iteration, LLR values in the reversed list change to the opposite signs and then starts decoding procedure until 30 iteration. Besides, the NLQ parameter γ uses 4.5 as simulation.

From the simulation result of Fig. 5.10, 0.2-0.3 dB performance enhancement is provided by the two-stage algorithm and has influence both on the LSD and bi-direction method. And there are a little comparison overhead to perform two-stage algorithm. Therefore, two-stage provides a method that could apply on all kinds of soft-output MIMO decoder to improve the performance.
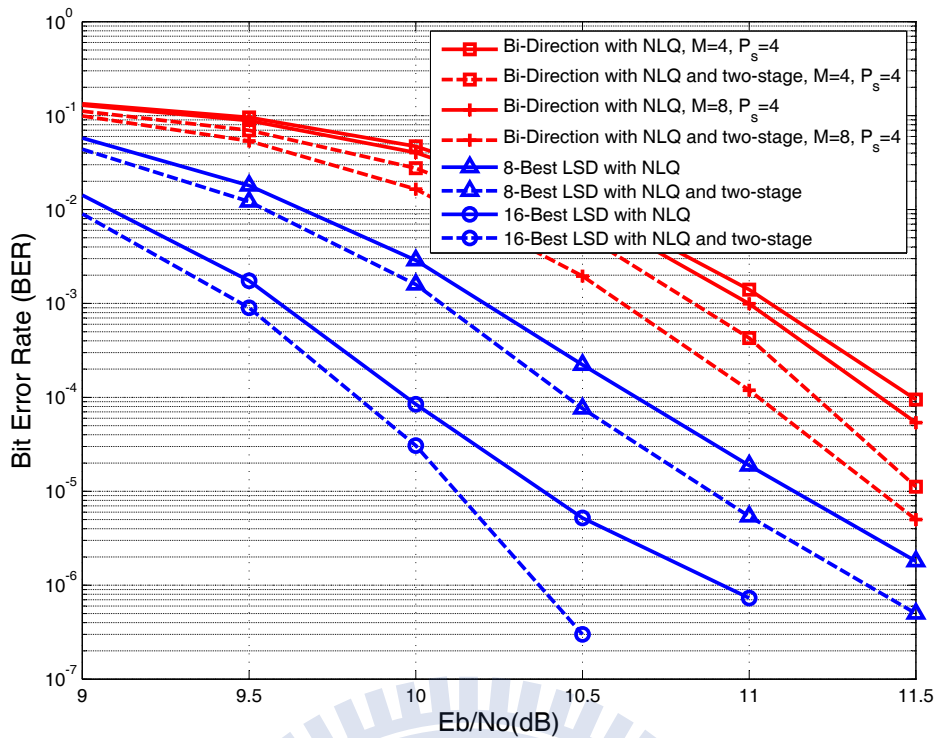
Figure 5.10: BER of $(2304, 1152)$ LDPC-coded 64-QAM 4×4 system, and $\gamma = 4.5$.

5.4   Summary

In conclusion, 64-QAM 4×4 MIMO system with $(2304, 1152)$ LDPC decoder is given as a summary. Fig. 5.11 shows that NLQ is applied on the LSD. For MIMO system without channel coding, that is, the hard decision of conventional K-Best sphere decoding, the parameter K should be chosen as 64 to approach ML solution. NLQ method applied on LSD could use the same K as the K-Best SD to achieve a great performance without any list expansion. And 64-Best LSD in the soft-output MIMO decoder is good enough when the NLQ method is performed.

QOC method indeed works better when M is small at Fig. 5.12. The performane of QOC for $M = 4$ achieves that of 16-Best LSD. However, the performane of QOC for $M = 32$ is worse than that of 32-Best LSD. And the complexity of QOC is higher than that of LSD in the same parameter. That is, the peformance of QOC is not increasing proportional to M, which is referred as the computation complexity. Therefore, the low complexity character of bi-direction method could be a replacement when M is increasing which is shown as Fig. 5.13.
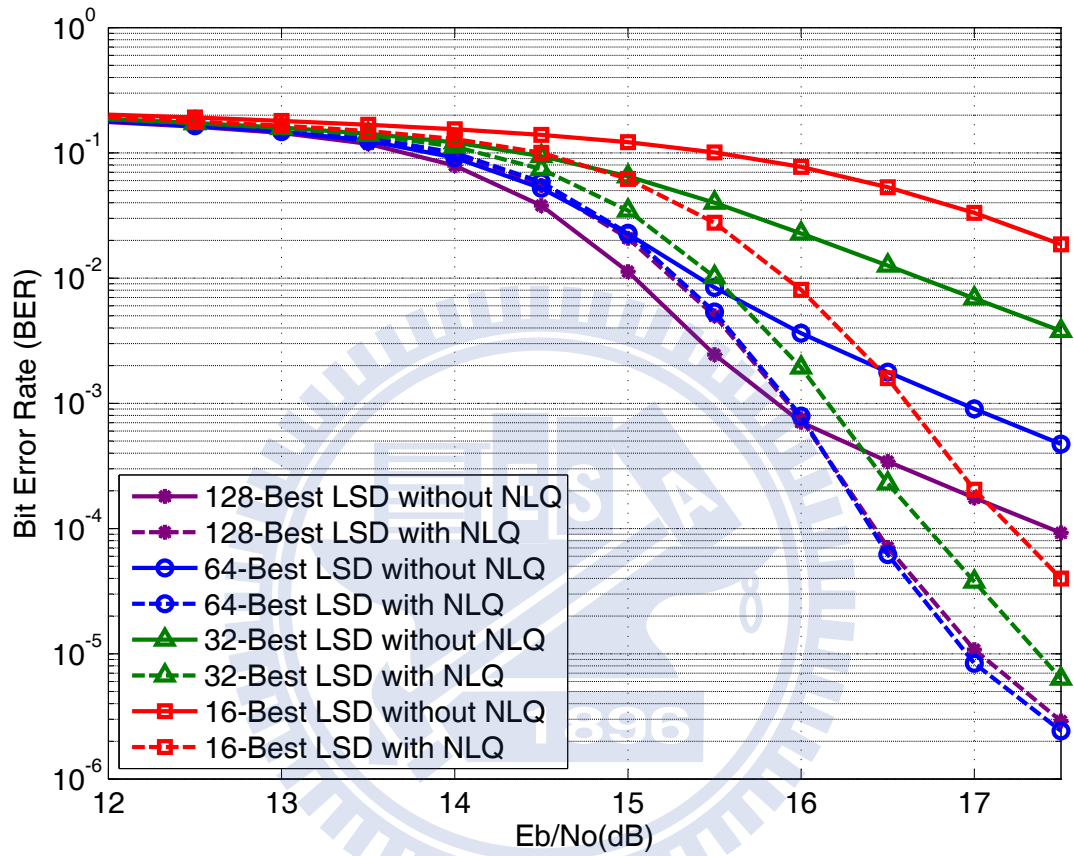
Figure 5.11: BER of $(2304, 1152)$ LDPC-coded 64-QAM 4×4 system after NLQ with $\gamma = 4.5$.
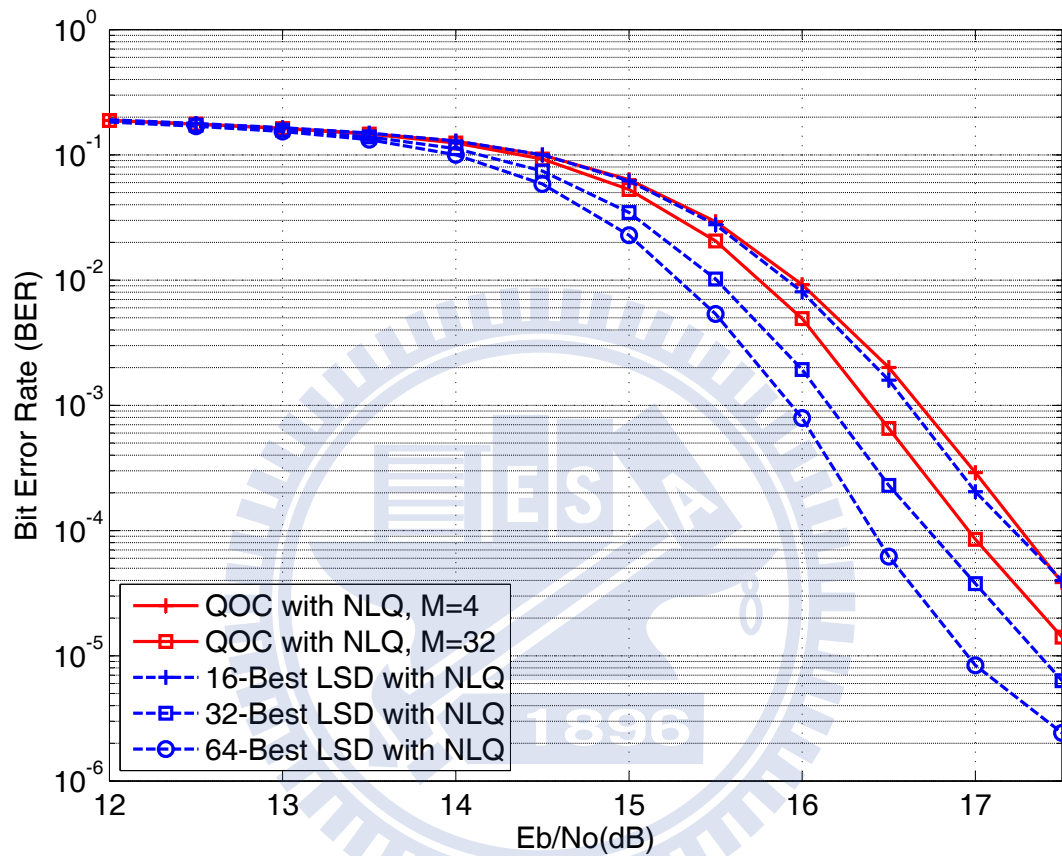
Figure 5.12: BER of $(2304, 1152)$ LDPC-coded 64-QAM 4×4 system after NLQ with $\gamma = 4.5$.

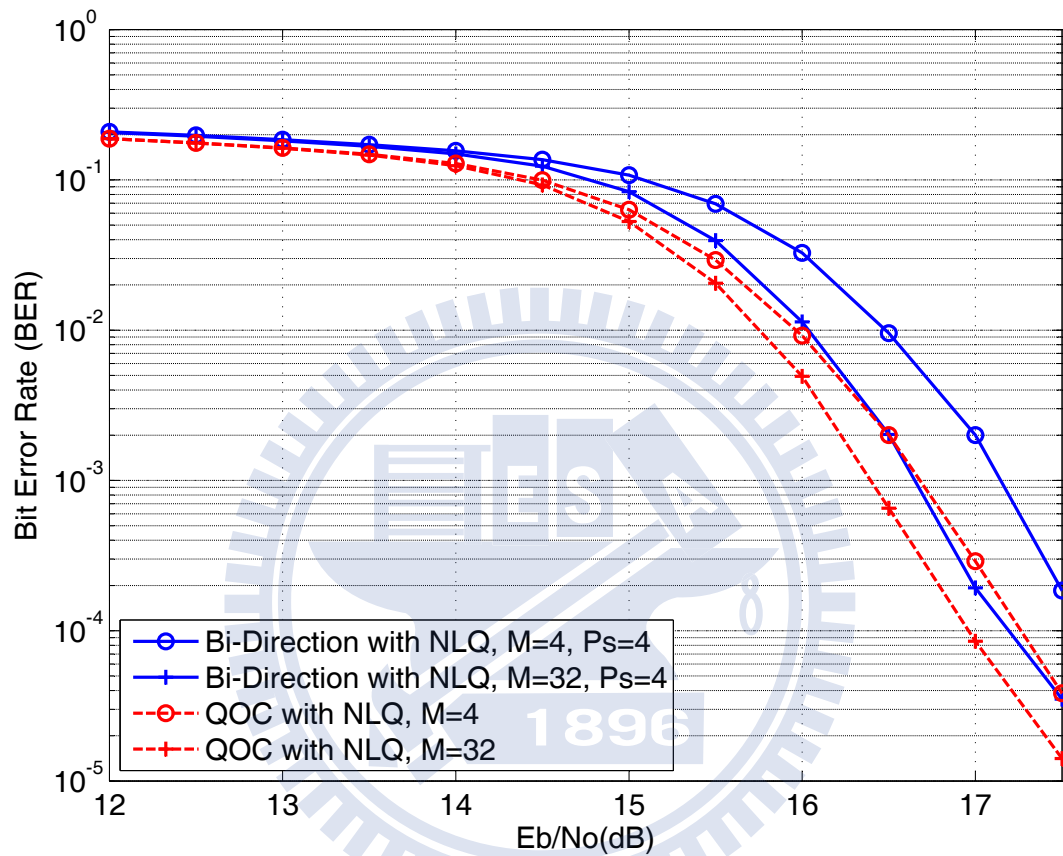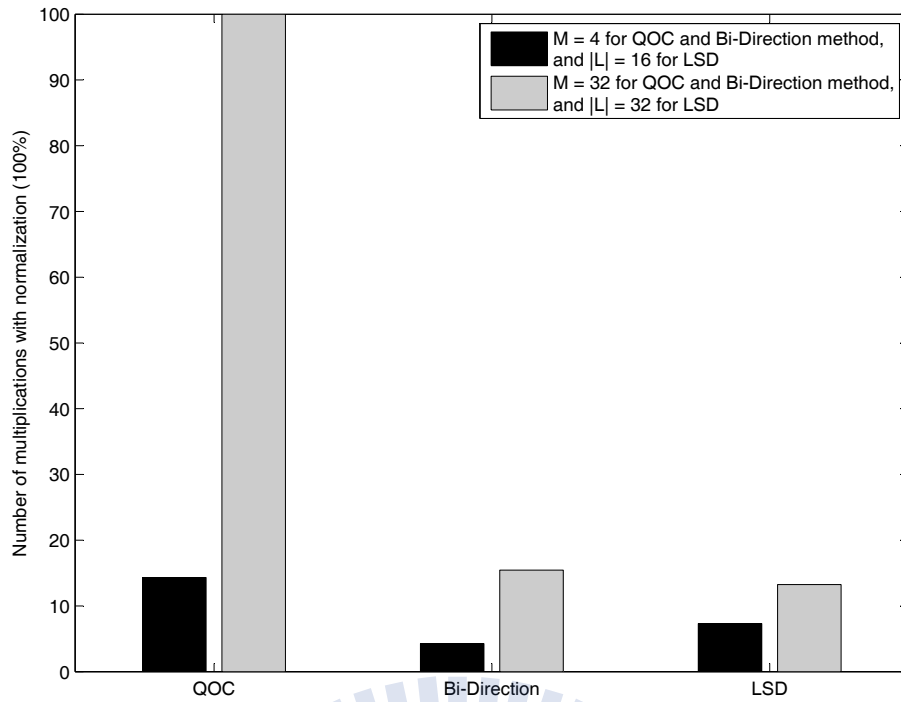Figure 5.13: BER of $(2304, 1152)$ LDPC-coded 64-QAM 4×4 system after NLQ with $\gamma = 4.5$.

Figure 5.14: Comparison of computation complexity in terms of multiplications.

From Fig. 5.13, the performance difference of bi-direction and QOC is smaller with the increasing of M. The performance loss is 0.5 dB for $M = 4$ and 0.2 dB for $M = 8$. And the computation complexity is analized as Fig. 5.14.

Chapter 6

Conclusion and Future Work

6.1 Conclusion

In this thesis, three methods are proposed to reduce the complexity and improve the performance for the channel-coded MIMO system. First, a bi-direction method reduces the complexity of the soft-output MIMO decoder. Traditionally, sphere decoder of the MIMO system encounters the empty-set issue as generating LLRs. Although the decoding method such as QOC solves the empty-set problem, the computation complexity is increasing intensively with the order of modulation and the list size. Bi-direction reduces computations by using two diagonal matrices and two decoding process and reduction is at most 30% compared to the original method QOC.

In addtion, nonlinear quantization (NLQ) is applied to the list sphere decoding and other soft-output MIMO decoder. By transforming the ouptut LLR distribution of MIMO detection, NLQ obtains a great performance improvement at most 2dB with little computation complexity. In the end, a two-stage algorithm for the channel-coded MIMO system is presented. An reversed list is constructed to store some unreliable bits from MIMO decoding. And the LLRs in the reversed list are changed to the opposite values as LDPC decoding procedure. The two-stage algorithm improves the bit error rate of the channel-coded MIMO decoder at most 0.3dB.

6.2 Future work

For the nonlinear quantiztion (NLQ), we use the same parameter $\gamma = 6$ in the whole simulation. However, the optimal value of γ maybe differ from the constellation, the size of the list at MIMO detection and channel decoding scheme. Therefore, a derivation of γ is essential in the future as a design parameter.

In addition, bi-direction could be applied on the other algorithms to reduce the comutation complexity with a few performance loss such as layered orthogonal lattice detector (LORD) [25] and list sphere decoding.

Bibliography

[1] A. J. Paulraj, D. A. Gore, R. U. Nabar, and H. Bolcskei, "An overview of MIMO communications - a key to gigabit wireless," in *Proc. IEEE*, vol. 92, no. 2, Feb. 2004, pp. 198–218.

[2] B. G. Evans and K. Baughan, "Vision of 4G," *Electron. Commun. Eng. J.*, vol. 12, no. 6, pp. 293–303, Dec. 2000.

[3] G. J. Foschini, "Layered space time architecture for wireless communicationin a fading environment when using multiple antennas," *Bell Lab. Tech. J.*, vol. 1, no. 2, pp. 41–59, Aug. 1996.

[4] S. Baro, J. Baro, and M. Witzke, "Iterative detection of MIMO transmission using a list-sequential (LISS) detector," in *IEEE International Conference on Communications (ICC)*, vol. 4, May 2003, pp. 2653–2657.

[5] H. Vikalo, B. Hassibi, and T. Hassibi, "Iterative decoding for mimo channels via modified sphere decoding," in *IEEE Trans. Wireless Commun.*, vol. 3, Nov. 2004, pp. 2299–2311.

[6] E. Viterbo and J. Boutros, "A universal lattice code decoder for fading channels," in *IEEE. Trans. Inf. Theory*, vol. 45, no. 5, Jul. 1999, pp. 1639–1642.

[7] K. W. Wong, C. Y. Tsui, R. S. K. Cheng, and W. H. Mow, "A VLSI architecture of a K-best lattice decoding algorithm for MIMO channels," *PIMRC*, vol. 02, 2002.

[8] E. Viterbo and J. Boutros, "A universal lattice code decoder for fading channels," *IEEE Trans. on Inform. Theory*, vol. 45, pp. 1639–1642, July. 1999.

[9] J. K. Winters, J. Salz, and R. D. Gitlin, "The impact of antenna diversity on the capacity of wireless communication systems," in *IEEE Trans. Commun.*, pp. 1740–1751.

[10] D. Tse and P. Viswanath, *Fundamentals of Wireless Communications.* New York: Cambridge University Press, 2005.

[11] P. W. Wolniansky, G. J. Foschini, G. D. Golden, and R. A. Golden, "V-blast: an architecture for realizing very high data rates over the rich-scattering wireless channel," in *IEEE International Conference on Signals, Systems and Electronics (ISSSE)*, Sep. 1994, pp. 295–300.

[12] E. Agrell, A. Vardy, and K. Zeger, "Closest point search in lattices," *IEEE Trans. on Inform. Theory*, vol. 48, no. 8, p. 2201V2214, Aug. 2002.

[13] Y.-H. Wu, Y.-T. Liu, H.-C. Chang, Y.-C. Liao, and H.-C. Chang, "Early-pruned K-best sphere decoding algorithm based on radius constraints," in *IEEE International Conference on Communications (ICC)*, pp. 4496–4500.

[14] H.-C. Chang, Y.-C. Liao, and H.-C. Chang, "Low-complexity prediction techniques of K-best sphere decoding for MIMO systems," in *IEEE Workshop on Signal Processing Systems*, pp. 45–49.

[15] C. Berrou and A. Glvieux, "Near optimum error correcting and decoding: Turbo-codes," in *IEEE Trans. Commun.*, pp. 1261–1271.

[16] R. G. Gallager, "Low-Density Parity-Check Codes," in *MA: MIT Press.*

[17] D. J. C.MacKay and R. M. Neal, "Near Shannon limit performance of low density parity check codes," *Electron. Lett*, vol. 33, no. 6, pp. 457–458, March 1997.

[18] B. M. Hochwald and S. ten Brink, "Achieving near-capacity on a multiple-antenna channel," in *IEEE Trans. Commun.*, vol. 51, Mar. 2003, pp. 389–399.

[19] T.-H. Im, I. Park, J. Kim, J. Yi, J. Kim, S. Yu, and Y.-S. Cho, "A new signal detection method for spatially multiplexed MIMO systems and its VLSI implementation," in *IEEE Trans. Circuits Syst. II: Express Briefs*, pp. 399–403.

[20] Y. Dai, S. Sun, and Z. Lei, "A comparative study of QRD-M detection and sphere decoding for MIMO-OFDM systems," *in Proc. IEEE Int. Symp.*, pp. 186–190, Sep. 2005.

[21] *Information technology-telecommunications and information exchange between systems-Local and metropolitan networks specific requirements-Part 11: wireless LAN medium access control (MAC) and physical layer (PHY) specifications: Enhancements for Higher Throughput,*, IEEE Std. Std. P802.11n.D1.0, 2006.

[22] *Local and metropolitan area network part16: air interface for fixed and mobile broadband wireless access systems draft*, IEEE Std. Std. P802.16e.D9, 2005.

[23] *Part 3: carrier sense multiple access with collision detection (CSMA/CD) access method and physical layer specifications amendment to IEEE Std 802.3-2005,*, IEEE Std. Std. P802.3an, 2006.

[24] M. P. C. Fossorier, M. Mihaljevic, and H. Imai, "Reduced complexity iterative decoding of low-density parity check codes based on belief propagation," in *IEEE Trans. Commun.*, vol. 47, May. 1999, pp. 673–680.

[25] M. Siti and M. P. Fitz, "A novel soft output layered orthogonal lattice detector for multiple antenna communications," in *IEEE International Conference on Communications (ICC)*, Jun. 2006, pp. 1686–1691.